Observational constraints on low redshift evolution of dark energy: How consistent are different observations?

H. K. Jassal,[1,*] J. S. Bagla,[1,†] and T. Padmanabhan[2,‡]

[1]*Harish-Chandra Research Institute, Chhatnag Road, Jhunsi, Allahabad 211 019, India*
[2]*Inter University Centre for Astronomy and Astrophysics, Post Bag 4, Ganeshkhind, Pune 411 007, India*
(Received 5 August 2005; published 4 November 2005)

The dark energy component of the Universe is often interpreted either in terms of a cosmological constant or as a scalar field. A generic feature of the scalar field models is that the equation of state parameter $w \equiv P/\rho$ for the dark energy need not satisfy $w = -1$ and, in general, it can be a function of time. Using the Markov chain Monte Carlo method we perform a critical analysis of the cosmological parameter space, allowing for a varying w. We use constraints on $w(z)$ from the observations of high redshift supernovae (SN), the Wilkinson Microwave Anisotropy Probe (WMAP) observations of cosmic microwave background (CMB) anisotropies, and abundance of rich clusters of galaxies. For models with a constant w, the ΛCDM(cold dark matter) model is allowed with a probability of about 6% by the SN observations while it is allowed with a probability of 98.9% by WMAP observations. The ΛCDM model is allowed even within the context of models with variable w: WMAP observations allow it with a probability of 99.1% whereas SN data allows it with 23% probability. The SN data, on its own, favors phantom-like equation of state ($w < -1$) and high values for Ω_{NR}. It does not distinguish between constant w (with $w < -1$) models and those with varying $w(z)$ in a statistically significant manner. The SN data allows a very wide range for variation of dark energy density, e.g., a variation by factor ten in the dark energy density between $z = 0$ and $z = 1$ is allowed at 95% confidence level. WMAP observations provide a better constraint and the corresponding allowed variation is less than a factor of 3. Allowing for variation in w has an impact on the values for other cosmological parameters in that the allowed range often becomes larger. There is significant tension between SN and WMAP observations; the best fit model for one is often ruled out by the other at a very high confidence limit. Hence results based on only one of these can lead to unreliable conclusions. Given the divergence in models favored by individual observations, and the fact that the best fit models are ruled out in the combined analysis, there is a distinct possibility of the existence of systematic errors which are not understood.

PACS numbers: 98.80.Es

INTRODUCTION

Observational evidence for accelerated expansion in the Universe has been growing in the last two decades [1]. Observations of high redshift supernovae [2,3] provided an independent confirmation. Using these along with observations of cosmic microwave background radiation (CMB) [4,5] and large scale structure [6,7], we can construct a "concordance" model for cosmology and study variations around it (e.g., see [5,8,9]; for an overview of our current understanding, see [10]).

Observations indicate that dark energy should have an equation of state parameter $w \equiv P/\rho < -1/3$ for the Universe to undergo accelerated expansion. Indeed, observations show that dark energy is the dominant component of our Universe. The cosmological constant is the simplest explanation for accelerated expansion [11,12] and it is known to be consistent with observations. In order to avoid theoretical problems related to cosmological constant [11], other scenarios have been investigated. In these models one can have $w \neq -1$ and in general w varies with redshift.

These models include quintessence [13], k-essence [14], tachyons [15,16], phantom fields [17], branes [18], etc. There is the Chaplygin gas model and its generalizations [19]. There are also some phenomenological models [20], field theoretical, and renormalization group based models (see e.g. [21]), models that unify dark matter and dark energy [22], and many others like those based on horizon thermodynamics (e.g. see [23]). Even though these models have been proposed to overcome the fine tuning problem for cosmological constant, most of these require similar fine tuning of parameter(s) to be consistent with observations. Nevertheless, they raise the possibility of $w(z)$ evolving with time (or being different from -1), which—in principle—can be tested by observations.

Given that $w < -1/3$ for dark energy for the Universe to undergo accelerated expansion, the energy density of this component changes at a much slower rate than that of matter and radiation. Indeed, $w = -1$ for cosmological constant and in this case the energy density is a constant. Unless w is a rapidly varying function of redshift and becomes $w \sim 0$ at ($z \lesssim 1$), the energy density of the dark energy component should be negligible at high redshifts ($z \gg 1$) as compared to that of nonrelativistic matter. If dark energy evolves in a manner such that its energy density is comparable to, or greater than the matter density

*Electronic address: hkj@hri.res.in
†Electronic address: jasjeet@hri.res.in
‡Electronic address: nabhan@iucaa.ernet.in

in the Universe at high redshifts then the basic structure of the cosmological model needs to be modified. We do not consider such models here. We confine our attention to models with dark energy density being an insignificant component of the Universe at $z \gg 1$ and choose observations which are sensitive to evolution of $w(z)$ at redshifts $z \lesssim 1$.

To put the present work in context, we recall that combining supernova observations with the WMAP data provides strong constraints on the variation of dark energy density [24]. (A review of relevant observations for constraining dark energy models along with a summary of the previous work in this area is given in Sec. II B.) Reproducing the location of acoustic features requires the angular diameter distance to the last scattering surface to be in the correct range. This analysis showed that while the data from SN observations allows for a large range in parameters of dark energy, combining with WMAP data limits this range significantly. However, in that work, we did not explore the cosmological parameter space widely and had fixed nearly all parameters other than those used to describe evolution of dark energy. In the present work, we allow many cosmological parameters to vary and include constraints from cluster abundance in addition to the supernova and WMAP constraints.

In addition to obtaining quantitative bounds on parameters in different contexts, we address the following key issues in this paper:

  (i) Does allowing cosmological parameters to vary weaken the constraints on variation of dark energy?
  (ii) Conversely, how does the allowed range for different cosmological parameters change when we allow for an epoch dependent $w(z)$?
  (iii) Do the observational constraints agree with each other? In particular, what kind of cosmological models are preferred by SN and WMAP observations individually?

The last point is important and requires elaboration. Different observational sets are combined together precisely because these observations are sensitive to different combinations of cosmological parameters and facilitate in breaking degeneracies between parameters. If we consider ΛCDM models then the SN observations, for example, broadly depend on the combination $(0.85\Omega_{\mathrm{NR}} - 0.53\Omega_V)$ [25] while WMAP is sensitive to $(\Omega_{\mathrm{NR}} + \Omega_V)$ [5], a feature which was originally highlighted in the literature as ''cosmic complementarity.'' Therefore, we cannot expect constraints from different observations to agree over the entire parameter space. At the same time, we do not expect models favored by one observation to be ruled out by another when such a divergence is not expected. This divergence may point to some shortcomings in the model, or to systematic errors in observations, or even to an incorrect choice of priors. If all observational sets are consistent then we should be able to derive similar constraints using subsets of observations, even though the final

constraints may not be as tight as with the full set of observations.

In order to address the questions listed above in a systematic manner, we proceed in three steps. We choose a ''base'' reference model with cold dark matter and cosmological constant, with neutrinos contributing a negligible amount to the energy density of the Universe. We assume that the Universe is flat and restrict ourselves to an unbroken power law for the primordial power spectrum of density fluctuations, and we assume that the perturbations are adiabatic. Another assumption is that the perturbations in tensor mode are negligible and we take $r = 0$ [26]. We choose this to be our standard model as this can be described by a compact set of parameters.

Next, we generalize from ΛCDM models ($w = -1$) to study a wider class of dark energy models with a *constant* w and address the issues listed above. In this case, we also study the effect of perturbations in dark energy. Finally, we generalize to models in which w is allowed to vary with z in a parameterized form. This approach allows us to delineate changes that come about from choosing a constant $w \neq -1$ from those allowed by a varying dark energy. We do not impose theoretically motivated constraints on models, e.g. we do *not* require $w \geq -1$ as the present work is focused on understanding the nature of models favored by observations.

The paper is organized as follows: In Sec. II we discuss the background cosmological equations followed by a brief review on the various observations used to constrain dark energy equation of state and the observations we concentrate on. The Markov Chain Monte Carlo method is discussed in Sec. III and detailed results are presented in Sec. IV. We conclude with a discussion of the results and future prospects for constraining dark energy models in Sec. V.

II. THEORETICAL BACKGROUND

A. Cosmological equations

If we assume that each of the constituents of the homogeneous and isotropic universe can be considered to be an ideal fluid, and that the space is flat, the Friedman equations become

$$\left(\frac{\dot{a}}{a}\right)^2 = \frac{8\pi G}{3}\rho, \tag{1}$$

$$\frac{\ddot{a}}{a} = -\frac{4\pi G}{3}(\rho + 3P), \tag{2}$$

where P is the pressure and $\rho = \rho_{\mathrm{NR}} + \rho_{\gamma} + \rho_{\mathrm{DE}}$ with the respective terms denoting energy densities for nonrelativistic matter, for radiation/relativistic matter and for dark energy. Pressure is zero for the nonrelativistic component, whereas radiation and relativistic matter have $P_{\gamma} = \rho_{\gamma}/3$.

If the cosmological constant is the source of acceleration then ρ_{DE} = constant and $P_{DE} = -\rho_{DE}$.

An obvious generalization is to consider models with a constant equation of state parameter $w \equiv P/\rho$ = constant. One can, in fact, further generalize to models with a varying equation of state parameter $w(z)$. Since a function is equivalent to an infinite set of numbers (defined e.g. by Taylor-Laurent series coefficients), it is clearly not possible to constrain the form of an arbitrary function $w(z)$ using a finite number of observations. One possible way of circumventing this issue is to parameterize the function $w(z)$ by a finite number of parameters and try to constrain these parameters by observations. There have been many attempts to describe varying dark energy with different parameterizations [24,27–31] where the functional form of $w(z)$ is fixed and the variation is described with a small number of parameters. Observational constraints depend on the specific parameterization chosen, but it should be possible to glean some parameterization independent results from the analysis.

To model varying dark energy we use two parameterizations

$$w(z) = w_0 + w'(z=0)\frac{z}{(1+z)^p}; \qquad p = 1, 2. \quad (3)$$

These are chosen so that, among other things, the high redshift behavior is completely different in these two parameterizations [24]. If $p = 1$ [32], the asymptotic value $w(\infty) = w_0 + w'(z=0)$ and for $p = 2$, $w(\infty) = w_0$. For both $p = 1, 2$, the present value is $w(0) = w_0$. Clearly, we must have $w(z \gg 1) \leq -1/3$ for the standard cosmological models with a hot big bang to be valid. This restriction is imposed over and above the priors used in our study.

Integrating $d(\rho a^3) = -w(z)\rho da^3$, the energy density can be expressed as

$$\frac{\rho_{DE}}{\rho_{DE_0}} = (1+z)^{3(1+w_0+w'_0)} \exp\left[-\frac{(3w'_0)z}{1+z}\right] \quad (4)$$

for $p = 1$ [in Eq. (3)] and

$$\frac{\rho_{DE}}{\rho_{DE_0}} = (1+z)^{3(1+w_0)} \exp\left[\frac{3w'_0}{2}\left(\frac{z}{1+z}\right)^2\right] \quad (5)$$

for $p = 2$. The allowed range of parameters w_0 and $w'_0 \equiv w'(z=0)$ is likely to be different for different p. However, the allowed variation at low redshifts in ρ_{DE} should be similar in both models as observations actually probe the variation of dark energy density. Indeed, in an earlier study [24] where we had studied a restricted class of models, we found this to be the case. For example, ρ_{DE} can vary by at most a factor 2 up to $z = 2$ when both the WMAP and SN data are taken into account [24]. This reaffirms the expectation that the results are parameterization independent at some level.

B. Observational constraints

In this subsection, we briefly review potential observational constraints on dark energy and we also summarize previous work in this area.

Constraints on dark energy models essentially arise as follows: To begin with, dark energy affects the rate of expansion of the Universe and thus the luminosity distance and also the angular diameter distance. Constraints from observations of high redshift supernovae [2,25,33–36] and the location of peaks in the angular power spectrum of CMB anisotropies mainly use this feature [37]. Gamma-ray bursts can be seen to much higher redshifts and if a subclass of these can be shown to be standard candle then we can probe distances and hence the evolution of dark energy over a wider range of redshifts [38]. The signature of acoustic peaks in correlation function of galaxies also provides a similar geometric constraint [39]. There is also an effect on gravitational lensing through changes in distance-redshift relation [40]. This change of distances has an effect on weak lensing statistics [41–45] and hence these also can be used as a probe of dark energy.

Second, the rate of expansion influences the growth of perturbations in the Universe and this leads to another set of probes of dark energy [46]. Abundance of rich clusters of galaxies, their evolution and the integrated Sachs-Wolfe (ISW) effect belong to this category of constraints, along with constraints from redshift space distortions [47–52]. All these constraints are sensitive to different aspects of dark energy and a combination of all of these can put tight limits on models. The redshift space distortions are a local effect as these are sensitive to the rate of growth of density perturbations at a given epoch. The abundance of rich clusters of galaxies, the ISW effect and distances are integrated effects in that the effect of dark energy is averaged over a range of redshifts in some sense.

Observations of high redshift supernovae of type Ia provide the most unambiguous evidence for accelerated expansion [2,25,33–35]. Assuming these sources to be standard candles, observations spanning a range of redshifts can be used to study the change in rate of expansion and this imposes direct constraints on the variation of dark energy density. Supernovae have been observed up to a redshift of $z_{max} \simeq 1.8$ and hence can be used to constrain models of dark energy up to this redshift. Constraints from SN observations alone however, permit a large variation in the dark energy parameters [35] and, in particular, favor models with $w < -1$ at the present epoch [3,25,34].

Baryon oscillations in the matter-radiation fluid prior to decoupling provide a standard scale and the angle at which the acoustic peaks occur in the angular power spectrum of temperature anisotropies in the CMB fixes the distance to the surface of last scattering. This provides a useful constraint on models of dark energy [37] as long as dark energy does not affect the dynamics of universe at the time of decoupling of matter and radiation. Unlike super-

novae that are observed over a range of redshifts where dark energy is dominant, the surface of last scattering is at $z \simeq 1100$. However, the exquisite quality of CMB anisotropy measurements makes this a very useful constraint and these observations offer a constraint that is different from SN observations [24]. Indeed, as we shall see, WMAP and SN observations often favor models that are mutually unacceptable.

Recent detection of the baryon acoustic peak in galaxy correlation function using the luminous red galaxy sample of the Sloan Digital Sky Survey (SDSS) survey has provided an additional handle to constrain cosmological parameters [39]. The geometric constraint from these observations can, in principle, constrain models of dark energy. A measurement of the angular scale corresponding to the peak at different redshifts can indeed be a powerful constraint.

If we consider a given cosmological model that is consistent with observations of CMB anisotropy then the amplitude of fluctuations at the time of decoupling is fixed, and its linearly extrapolated value today can be computed using linear perturbation theory. The abundance of rich clusters of galaxies is related to the amplitude of perturbations in dark matter at a scale of about $8 \ h^{-1}$ Mpc. If we study different models for dark energy while other parameters are not changed, the abundance of rich clusters constrains the net growth of structures between the epoch of decoupling and the present epoch [53].

Redshift space distortions due to kinematics and the Alcock-Paczynski effect are also potential probes of dark energy [51,54]. Ongoing surveys like the SDSS and future surveys will be able to distinguish between different dark energy models through these effects [55]. However, this method does not provide useful constraints at present.

Dependence of the distance-redshift relation and a different rate of growth for perturbations, as well as changes in the matter power spectrum, are also reflected in weak lensing statistics. Several studies have been carried out on the potential constraints that can be put on dark energy models from weak lensing observations and their degeneracy with other parameters. These studies indicate that future surveys will be able to put strong constraints on dark energy models [42,44].

Growth of perturbations also leaves a signature in the CMB anisotropy spectrum at large angular scales. The ISW effect leads to an enhancement in the angular power spectrum at these scales. The detailed form of this enhancement depends on the equation of state parameter w and its variation. This effect can be detected by cross correlation of temperature anisotropies with the foreground distribution of matter [56]. It is difficult to distinguish the ISW effect from the effect of a small but nonzero optical depth τ due to reionization by using only the temperature anisotropies in the CMB; cross correlation with the matter distribution or polarization anisotropies in the CMB must be used.

Redshift surveys of galaxy clustering do not constrain properties of dark energy directly; however, the shape of the power spectrum constrains the combination $\Gamma = \Omega_{NR}h$ [57]. This provides an indirect constraint on dark energy through the well-known degeneracy between Ω_{NR} and w_0 (e.g. see [24]).

The large number of different observations that can be used to constrain dark energy models is encouraging. Indeed, many attempts have been made to use some of these observations to put constraints on models [9,24,27,53,58].

C. A choice of three observations

In this work, we concentrate on SN, WMAP and cluster abundance observations. We briefly explain the reason for this choice and the kind of constraints one can expect.

The left panel in Fig. 1 shows the degeneracy in Ω_{NR} and w_0 [for models with constant w; i.e., with $w'_0 = 0$ in Eq. (3)]. The figure shows contours of constant luminosity distance $H_0 d_l(z)$ at $z = 0.17$ (solid curves) and $z = 1.17$ (dashed curves). The second panel displays the constant luminosity distance contours in the $w'(z = 0) - w_0$ plane for $p = 2$ if $\Omega_{NR} = 0.3$. Given that SN observations constrain luminosity distance as a function of redshifts, these figures illustrate the shape of the allowed region that we are likely to get and also demonstrate the degeneracies between different parameters. The third panel shows how the redshift at which the expansion of the Universe begins to accelerate depends on the parameters w_0 and $w'(z = 0)$ for $p = 2$. This epoch is constrained by SN observations and hence the allowed region in parameter space should lie between contours of this nature. Clearly, regions with a late onset of acceleration (upper right corner) as well as a very early onset of acceleration (lower right corner) will be ruled out by observations of supernovae.

The fourth panel of this figure shows the redshift at which matter and dark energy contribute equally in terms of the energy density of the Universe. Structure formation constraints are likely to follow these contours as the rate of growth for density perturbations is significant only in the matter dominated era. Too little structure formation (upper right corner) as well as too much structure formation (lower left corner) are likely to restrict the allowed models along a diagonal (upper left to lower right) in this plane.

Lastly, the location of acoustic peaks in the angular power spectrum of temperature anisotropies in the CMB is the most significant constraint provided by CMB observations. This essentially constrains the distance to the surface of last scattering and hence a suitably defined [see Eq. (8)] mean value (w_{eff}) for w. The right panel shows contours of w_{eff}, which run almost diagonal in this plane. Thus a band of allowed models is the likely outcome of comparison with observations. The contours of w_{eff} are the same as contours of equal distance to the surface of last
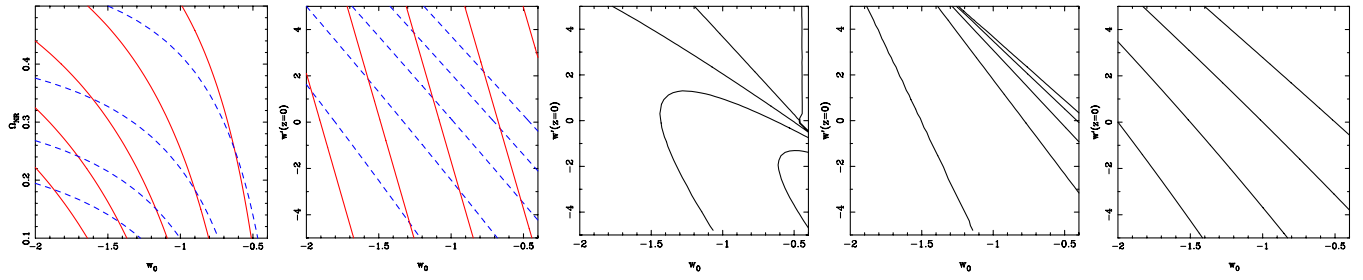
FIG. 1 (color online).   The left figure in this panel shows contours of constant luminosity distance $H_0 D_L(z)/c$ in $\Omega_{\rm NR} - w$ plane. The solid contours are for luminosity distance at redshift $z = 0.17$ and the dashed ones are for luminosity distance at redshift $z = 1.17$. The solid contours from top right to bottom left correspond to values between $H_0 D_L(z = 0.17)/c = 0.19 - 0.21$ and the dashed lines are for $H_0 D_L(z = 1.17)/c = 1.52 - 2.45$. The other plots show contours in the $w_0 - w'(z = 0)$ plane. The second figure shows contours of constant $H_0 D_L(z = 0.17)/c$ and $H_0 D_L(z = 1.17)/c$. Starting from upper right the contours are for $H_0 D_L(z = 0.17)/c = 0.18 - 0.2$ and $H_0 D_L(z = 1.17)/c = 1.63 - 2.1$. The third panel shows contours of redshift at which the expansion of the Universe starts to accelerate. Starting from the upper right corner in a counterclockwise direction, the contours are for $z = 0, 0.2, 0.4, 0.6$, and 0.8. The constraint from SN observations essentially constrains this redshift and hence the allowed region can be expected to follow these contours. The next panel shows redshift at which the energy density in matter and dark energy are equal. The curves, starting from the left are for $z = 0.2, 0.4, 0.6, 0.8$, and 1.0. Structure formation constraints are likely to follow these contours as the rate of growth for density perturbations is significant only in the matter dominated era. The right panel shows contours of $w_{\rm eff}$ at the surface of last scattering [see Eq. (8)]. From top right towards bottom left the values are $w_{\rm eff} = -0.5, -1.0, -1.5$, and -2.0 If the location of acoustic peaks provides the main constraint then the region allowed by CMB observations should follow these contours. We have used $\Omega_{\rm NR} = 0.3$ for these plots.

scattering, or the l corresponding to the first peak in the angular power spectrum of CMB temperature fluctuations.

SN data provides geometric constraints for dark energy evolution. These constraints are obtained by comparing the predicted luminosity distance to the SN with the observed one. The theoretical model and observations are compared for luminosity measured in magnitudes:

$$m_B(z) = \mathcal{M} + 5\log_{10}(D_L), \qquad (6)$$

where $\mathcal{M} = M - 5\log_{10}(H_0)$ and $D_L = H_0 d_L$; M being the absolute magnitude of the object and d_L is the luminosity distance

$$d_L = (1 + z)a(t_0)r(z); \qquad r(z) = c\int \frac{dz}{(1 + z)H(z)}, \quad (7)$$

where z is the redshift. This depends on evolution of dark energy through $H(z)$. For our analysis we use the combined *gold* and *silver* SN data set in [3]. This data is a collection of supernova observations from [2,33] and many other sources with 16 supernovae discovered with Hubble space telescope [3]. The parameter space for comparison of models with SN observations is small and we do a dense sampling of the parameter space.

CMB anisotropies constrain dark energy in two ways—through the distance to the last scattering surface and through the ISW effect. Given that the physics of recombination and evolution of perturbations does not change if $w(z)$ remains within some *safe limits*, any change in the location of peaks will be due to dark energy [37]. The angular size θ of the Hubble radius at the time of decoupling can be written as

$$\theta^{-1} = \frac{H(z)/H_0}{\int_0^z dy/(H(y)/H_0)}$$

$$\simeq \frac{\sqrt{\Omega_{\rm NR}(1 + z)^3}}{\int_0^z dy/\sqrt{\Omega_{\rm NR}(1 + z)^3 + \varrho^{\rm DE}(z)/\varrho_0^{\rm DE}}}$$

$$\equiv \frac{\sqrt{\Omega_{\rm NR}(1 + z)^3}}{\int_0^z dy/\sqrt{\Omega_{\rm NR}(1 + z)^3 + \Omega_{\rm DE}(1 + z)^{3(1+w_{\rm eff})}}}. \quad (8)$$

The second line is obtained as decoupling happens at a redshift where dark energy is not important, and if we ignore the contribution of radiation and relativistic matter; the last equation defines $w_{\rm eff}$. Clearly, the value of the integral will be different if we change w_0, $w'(z = 0)$ and there also will be some dependence on the parameterized form. Location of peaks in the angular power spectrum of the CMB provide a constraint, but this can only constrain $w_{\rm eff}$ and not all of w_0, $w'(z = 0)$ and p. Therefore if the present value $w_0 < w_{\rm eff}$ then it is essential that $w'(z = 0) > 0$, and similarly if $w_0 > w_{\rm eff}$ then $w'(z = 0) < 0$ is needed to ensure that the integrals match. Specifically, the combination of w_0, $w'(z = 0)$ and p should give us a $w_{\rm eff}$ within the allowed range.

In our analysis, we use the angular power spectrum of the CMB temperature anisotropies [59,60] as observed by WMAP, and these are compared to theoretical predictions using the likelihood program provided by the WMAP team [61]. We vary the amplitude of the spectrum till we get the best fit with WMAP observations. Note that this is different from the commonly used approach of normalizing the

angular power spectrum at $l = 10$. As we use the entire angular power spectrum for comparison with observations, the impact of ISW effect on the likelihood is relatively small.

It has been pointed out that constraints from structure formation restrict the allowed variation of dark energy in a significant manner [53]. We use observed abundance of rich clusters [47–49] to apply this constraint. Since the mass of a typical rich cluster corresponds to the scale of $8 \ h^{-1}$ Mpc, cluster abundance observations therefore constrain σ_8, the rms fluctuations in density contrast at $8 \ h^{-1}$ Mpc. The number density of clusters depends strongly on σ_8 and Ω_{NR}. We use the σ_8 constraints given in [47] from ROSAT deep cluster survey and are given by $\sigma_8 = (0.58 \pm 0.1) \times \Omega_{NR}^{-0.47+0.16\Omega_{NR}}$ at 99% confidence level. The cosmological model should predict σ_8 in the allowed range in order to be consistent with observations.

Recent detection of the baryon acoustic peak using luminous red galaxy sample of the SDSS survey has provided an additional handle to constrain the cosmological parameters [39]. We also used distance scale D_V at redshift $z = 0.35$ introduced in the above reference to further constrain the cosmological models. Here $D_V(0.35)^3 \equiv D_M(z)^2 cz/H(z)$ and the observational constraint is $D_V(0.35) = 1370 \pm 64$ Mpc at the 1σ level. This fourth observation does not add significantly to other constraints listed here and we will not describe quantitative results from this constraint here.

Priors used in the present study are listed in Table I. Apart from the limits on the models studied here, we also assumed that neutrinos are massless and the ratio r of tensor to scalar mode is zero. These assumptions are consistent with the known upper bounds, and in any case these do not make any difference to the observations used here as constraints [26].

TABLE I. This table lists the priors used in the present work. Apart from the range of parameters listed in the table, we assumed that the Universe is flat. We assumed that the primordial power spectrum had a constant index. Further, we ignored the effect of tensor perturbations. The range of values for w_0 and $w'(z = 0)$ is as given below, but with the constraint that $w(z = 1000) \leq -1/3$. Any combination of w_0 and $w'(z = 0)$ that did not satisfy this constraint was not considered.

Parameter	Lower limit	Upper limit
Ω_B	0.03	0.06
Ω_{NR}	0.1	0.5
h	0.6	0.8
τ	0.0	0.4
n	0.86	1.10
w_0	-2.0	-0.4
$w'(z = 0)$	-5.0	5.0

III. MARKOV CHAIN MONTE CARLO METHOD

We compute χ^2 using the routines provided by the WMAP team [61]. The CMBFAST package [62] is used for computing the theoretical angular power spectrum for a given set of cosmological parameters. We have combined the likelihood program with the CMBFAST code, and this required a few minor changes in the CMBFAST driver routine. Given the large number of parameters, the task of finding the minimum χ^2 and mapping its behavior in the entire range of values for parameters is computationally intensive.

We adapt the Metropolis algorithm [63] (also known in the context of parameter estimation as the Markov Chain Monte Carlo method [61,64]) for efficiently mapping regions with low values of χ^2. The algorithm used is as follows:

(1) Start from a random point $\mathbf{r}_i$ in parameter space and compute C_l and $\chi^2(\mathbf{r}_i)$.
(2) Consider a small random displacement $\mathbf{r}_{i+1} = \mathbf{r}_i + d\mathbf{r}$ and compute $\chi^2(\mathbf{r}_{i+1})$.
(3) If $\chi^2(\mathbf{r}_{i+1}) \leq \chi^2(\mathbf{r}_i)$ then $i \rightarrow i + 1$. Go to the first step.
(4) Else:
  (a) Compute $\Delta\chi^2 = \chi^2(\mathbf{r}_{i+1}) - \chi^2(\mathbf{r}_i)$ and $\exp[-\alpha\Delta\chi^2]$.
  (b) Compare this with a random number $0 \leq \beta \leq 1$.
  (c) If $\beta \leq \exp[-\alpha\Delta\chi^2]$ then $i \rightarrow i + 1$. Go to the first step.

The size of the small displacement $d\mathbf{r}$ and the parameter α are chosen to optimally map the regions of low χ^2. We wish the chain to converge towards the minimum, starting from an arbitrary point, and we also want the Markov chain to map the region in parameter with low χ^2 exhaustively without getting bogged down near the minima. These two conflicting requirements are reconciled by choosing a small but nonzero value of α. Maximum displacement allowed in one step is small compared with the range of parameters, but not small enough for the chain to get trapped in a small region around the minimum. The optimum values of maximum displacement and α are related to each other. We ran several chains with a varying number of points; a typical chain has about 10^4 points. For each set, we have at least 10^5 points. [We have done calculations for five sets: cosmological constant, constant w with and without perturbations in dark energy, time varying $w(z)$ for $p = 1$ and $p = 2$. Results presented here required an aggregate CPU time of nearly 10 000 h on 2.4 GHz Xeon CPUs]. The convergence criteria for such chains is satisfied for all the sets and for all the parameters in each set [65].

We use the Markov Chain Monte Carlo approach only for comparison of models with the CMB data. Observations of cluster abundance are compared with models from the Markov chain run for CMB, after the chain has been run. Comparison of models with observations of high

redshift supernovae is done separately. This approach is more conducive to one of the questions that we wish to address, namely, are the observational constraints consistent with each other?

IV. RESULTS

We present results in the form of likelihood functions for various parameters in sets of increasing complexity, starting with the standard ΛCDM model. Before we proceed with a discussion of results in this form, we discuss a few specific models sampling a few interesting regions of the parameter space in order to develop an intuitive feel for different observational constraints. We call these fiducial or reference models. Along with the fiducial models, we also discuss the best fit models in each set. We find the best fit model for individual observations as well as for the combination of all the observations.

A. Fiducial models

1. The ΛCDM model

The ΛCDM model is our "standard" model and we begin our discussion with this class of models. Several studies have been carried out to constrain parameters for the ΛCDM model [5,9]. Our results for the ΛCDM model bring out—among other things—the differences from previous work which arises due to a different method we use here for normalizing power spectra. (See Sec. II C for details.) Differences introduced by priors are also apparent. Our results are as follows:

(i) For the ΛCDM model, if we consider SN observations alone, we get a best fit at $\Omega_{\rm NR} = 0.28$ with a $\chi_S^2 = 233.1$. (We will use subscript S for χ^2 from SN analysis and W for analysis with WMAP observations.) This model with $\Omega_{\rm NR} = 0.28$ is allowed by WMAP observations and has a best fit $\chi_W^2 = 974.3$ for $\Omega_B = 0.045$, $h = 0.69$, $n = 0.95$, and $\tau = 0.008$. SN observations do not fix these parameters so we varied the other parameters to get the best fit WMAP model for $\Omega_{\rm NR} = 0.28$.

(ii) The model which best fits the WMAP observations has $\Omega_B = 0.05$, $\Omega_{\rm NR} = 0.34$, $h = 0.66$, $n = 0.96$, and $\tau = 0.002$ with a $\chi_W^2 = 972.5$. The χ^2 value corresponding to SN fit is $\chi_S^2 = 239.9$. In the context of cosmological constant models alone, this model is away from the SN best fit by $\Delta \chi_S^2 = 6.8$ and is allowed with probability 0.009. In other words, the model most favored by WMAP observations is allowed by the SN observations only with less than 1% probability. (We define probability $\mathcal{P}$ of a given model to be $1 - C/100$, where $C\%$ is the confidence limit at which the model is allowed. By using this definition we avoid dilution due to a large parameter space. While the statement about χ^2 is accurate and directly obtainable from the analysis,

the conversion of confidence intervals to probabilities has well-known statistical caveats while dealing with multiparameter fits. This should be kept in mind while interpreting our statements about probability with which a model is allowed). In contrast, the model most favored by SN observations is allowed by WMAP observations with a probability of $\mathcal{P} = 0.945$.

We now restrict some of the parameters to values favored by other observations e.g. [66]. We fix the baryon density parameter $\Omega_B = 0.05$, present day Hubble parameter $h = 0.7$, and the spectral index $n = 1$ for these models. Allowing $\Omega_{\rm NR}$ and τ to vary the best fit ΛCDM model in this restricted class of models is with $\Omega_{\rm NR} = 0.31$ and $\tau = 0.14$ and $\chi_W^2 = 974.8$. This is fairly close to the best fit model found by the WMAP team using a large set of observations [5]. This model is allowed by the rich cluster abundance observations, and also by SN observations ($\chi_S^2 = 234.8$, the corresponding probability being $\mathcal{P} = 0.2$).

Thus convergence between the WMAP and SN observations happens *only* in a narrow window for flat ΛCDM models, with the SN constraint being the tighter of the two. It is worth mentioning that in a wider class of models, (obtained by relaxing the prior $\Omega_{\rm tot} = 1$) SN data favors a closed universe with $\Omega_{\rm tot} = 1.44 \pm 0.28$ and—more importantly—allows the $\Omega_{\rm tot} = 1$ models with $\mathcal{P} = 0.12$ [25].

2. Models with a constant w

We now allow the dark energy equation of state parameter to have values different from $w = -1$ but do not allow variation with time. We then find that

(i) SN observations favor a model with $w = -1.99$ and $\Omega_{\rm NR} = 0.47$ and with $\chi_S^2 = 227.5$. This is the root cause of the phantom menace. This model is, however, ruled out at a very high probability by WMAP data (with a $\Delta \chi_W^2 = 13.6$) and is allowed only with $\mathcal{P} = 0.022$.

(ii) WMAP observations favor higher values for w (nonphantom models) and the best fit model has $w = -0.72$. The other cosmological parameters corresponding to this best fit are $\Omega_B = 0.06$, $\Omega_{\rm NR} = 0.34$, $h = 0.64$, $n = 0.99$, and $\tau = 0.19$ with $\chi_W^2 = 971.6$. SN observations, on the other hand, rule out this model at a very high significance level ($\Delta \chi_S^2 \simeq 53$). This is the case when we do not take perturbations in dark energy into account for computing theoretical predictions.

(iii) If we include dark energy perturbations [67] the model which fits best with WMAP observations is the same as the best fit for the ΛCDM models. This model is allowed by SN observations with $\chi^2 = 239.3$ which is allowed with probability 0.003. Clearly, the discrepancy between the WMAP and

SN observations is reduced when we take perturbations in dark energy into account, but SN observations allow the WMAP best fit model only marginally even in this case.

(iv) How well does the ΛCDM fare when we allow a range of w? The cosmological constant is allowed with $\mathcal{P} = 0.063$ by SN observations in the set of models with constant w. WMAP observations allow the ΛCDM models with a very high probability, indeed the best fit model continues to be a ΛCDM model if perturbations in dark energy are taken into account.

To illustrate these aspects, we consider two fiducial models with $w = -1.5$ and $w = -0.9$ allowing $\Omega_{\rm NR}$ and τ to vary. Other parameters are fixed as for the ΛCDM model (see subsection IV A 1 above). We do not take perturbations in dark energy into account here. The best fit values using WMAP observations for $w = -1.5$ are $\Omega_{\rm NR} = 0.38$ and $\tau = 0.04$. Generically, models with lower w require higher values of $\Omega_{\rm NR}$, which is clear from the form of the curves in Fig. 1(a). This model is allowed by WMAP observations with $\chi^2_W = 978.8$ as well as by SN observations ($\chi^2_S = 229.9$). But this model is *not* allowed by observations of cluster abundance. The value of $\sigma_8 = 1.1$ for this model is higher than the upper limit $\sigma_8 = 1.02$ allowed with 99% confidence level for this value of $\Omega_{\rm NR}$.

With $w = -0.9$, WMAP favors a model with $\Omega_{\rm NR} = 0.28$ and $\tau = 0.18$ ($\chi^2_W = 974.5$). This model is allowed by cluster abundance observations. The model becomes marginal when SN observations are taken into account with $\chi^2_S = 237.9$, as compared to a minimum of $\chi^2_S = 227.5$ for models with constant w.

Once again, we find that WMAP observations and SN observations favor different regions in the parameter space. Generalizing to the class of models with a constant w from $w = -1$, we find that SN data has a distinct preference for $w < -1$ and the ΛCDM model is allowed only marginally. WMAP data also shows a mild preference for models with $w \neq -1$, though it continues to allow the ΛCDM model. If perturbations in dark energy are taken into account then the ΛCDM model continues to be the most favored model for WMAP observations.

3. Models with varying $w(z)$

Next, we allow the dark energy equation of state parameter to vary. As it is not possible to take the effect of nonadiabatic perturbations into account for these models and as we do not wish to add another parameter, we work with models without any perturbations in dark energy [68]. It is clear that this will introduce a slight bias towards models with $w > -1$ but will not change anything else. For the discussion of fiducial models, we choose the parameterization with $p = 2$ in Eq. (3).

(i) Parameter values for the best fit model with SN data are $w_0 = -1.95$, $w'(z = 0) = -4.5$, and $\Omega_{\rm NR} = 0.498$ with a $\chi^2_S = 227.4$. As with the constant w models, SN data favors large negative values of the equation of state parameter. *SN observations do not favor models with varying $w(z)$ over models with $w \neq -1$, since the change in best fit χ^2 is only 0.1 when the additional parameters are added.* WMAP observations allow this model with $\mathcal{P} = 0.035$ ($\chi^2_W = 987.6$) if we have $\Omega_B = 0.056$, $h = 0.662$, $n = 1.04$, and $\tau = 0.002$. However, this model is ruled out by cluster abundance observations as $\sigma_8 = 1.25$ for this model is higher than the allowed range at 99% confidence level.

(ii) The best fit model for WMAP data has $w_0 = -1.48$, $w'(z = 0) = 3.86$, $\Omega_B = 0.05$, $\Omega_{\rm NR} = 0.24$, $h = 0.73$, $n = 1.1$, and $\tau = 0.35$ with $\chi^2_W = 970.9$. This model is allowed by SN observations with $\mathcal{P} = 0.33$ ($\Delta\chi^2 = 4.63$).

The tension between the WMAP and SN observations is less serious for models with varying w than for models with a constant w. Part of the reason is that with a larger number of parameters, the same $\Delta\chi^2_S$ gives us a larger probability for a given model.

As in the previous cases, let us choose fiducial models by restricting some of the parameters. We consider a model with dark energy parameter values $w_0 = -1.5$ and $w'(z = 0) = 1.0$. The WMAP best fit with these parameters is with $\Omega_{\rm NR} = 0.37$ and $\tau = 0.0005$ with $\chi^2_W = 976.5$. The change in acceptance level of this model is due to our restricting the values of the spectral index and the Hubble parameter. This model has $\chi^2_S = 229.3$ and is allowed by all the three observations used here.

If we move closer to the model most favored by SN observations, $w_0 = -1.5$ and $w'(z = 0) = -5.0$, then we find that WMAP data favors $\Omega_{\rm NR} = 0.42$ and $\tau = 0.0$. Even this model is outside the range allowed by WMAP observations at 68% confidence limit and is allowed at $\mathcal{P} = 0.12$. The model fares similarly with SN observations, i.e., it is allowed with $\mathcal{P} = 0.12$.

We wrap up with a discussion of a model with $w_0 > -1$. We consider $w_0 = -0.9$ and $w'(z = 0) = -3.0$. WMAP observations allow this model with $\chi^2_W = 977.4$ for $\Omega_{\rm NR} = 0.365$ and $\tau = 0.0013$. SN observations allow this model within the 95% confidence limit with a probability $\mathcal{P} = 0.15$. This model is also allowed by observations of cluster abundance.

Within the context of models with a variable $w(z)$, the ΛCDM model is allowed by WMAP observations ($\Delta\chi^2_W = 1.6$) as well as by supernova observations ($\Delta\chi^2_S = 5.73$). SN observations clearly favor models other than the ΛCDM model in context of $\Omega_{\rm tot} = 1$, while no such preference is seen for WMAP observations. However, models favored by SN observations require $\Omega_{\rm NR}$ to be much larger than the values favored by observations of rich clusters [1].

In summary, there is significant tension between the sets of observations we are studying and this tension does not

TABLE II.   This table lists best fit parameter values and χ^2 for different models and some of the selected fiducial models. The abbreviation b.f. denotes the best fit model for the particular data set. The corresponding probabilities are given in brackets.

		Ω_B	h	n	τ	Ω_{NR}	w	w'	$\chi^2_W(P)$	$\chi^2_S(\mathcal{P})$
ΛCDM	WMAP(b.f.)	0.05	0.663	0.96	0.002	0.34	-1		972.5	239.9 (0.009)
	SN(b.f.)	0.045	0.697	0.95	0.008	0.28	-1		973.7 (0.94)	233.1
	model 1	0.05	0.70	1.0	0.14	0.31	-1		971.8 (0.8)	234.8 (0.21)
$w = $ constant	WMAP(b.f.)	0.06	0.635	0.99	0.19	0.34	-0.72		971.6	280.0 ($<$0.001)
	SN(b.f.)	0.055	0.666	1.0	0.05	0.47	-1.99		985.2 (0.022)	227.46
	model 1	0.05	0.70	1.0	0.04	0.38	-1.5		978.8 (0.314)	229.9 (0.299)
	model 2	0.05	0.70	1.0	0.18	0.28	-0.9		974.5 (0.82)	237.9 (0.005)
$w = $ constant	WMAP(b.f.)	0.05	0.664	0.95	0.0	0.32	-0.96		972.8	239.3 (0.003)
with perturbations	SN(b.f.)	0.055	0.666	1.0	0.05	0.47	-1.99		985.2 (0.022)	227.46
	model 1	0.05	0.70	1.0	0.06	0.38	-1.5		979.2 (0.395)	229.9 (0.299)
	model 2	0.05	0.70	1.0	0.16	0.28	-0.9		976.1 (0.77)	237.9 (0.005)
$p = 2$	WMAP(b.f.)	0.05	0.73	1.1	0.35	0.24	-1.48	3.86	970.9	232.1 (0.33)
	SN(b.f.)	0.056	0.662	1.04	0.002	0.498	-1.95	-4.5	987.6 (0.035)	227.37
	model 1	0.05	0.70	1.0	0.0005	0.37	-1.5	1.0	976.5 (0.692)	229.3 (0.75)
	model 2	0.05	0.70	1.0	0.0	0.42	-1.5	-5.0	983.8 (0.123)	234.9 (0.116)
	model 3	0.05	0.70	1.0	0.0013	0.365	-0.9	-3.0	977.4 (0.56)	234.4 (0.147)

reduce when the parameter space is enlarged. We see that best fit model for one set of observation is often ruled out by another set with a high level of significance. There is an overlap of region allowed with 95% confidence limit in all cases and within 68% confidence limit in some cases; but this does not take away the significance of the differences which the above analysis has given. The results presented here are summarized in Table II.

B. Results in detail

In this section we outline the detailed results of our analysis. We marginalize the results in the multidimensional parameter space to derive likelihood function for each parameter of interest. The likelihood function is sensitive to the bin size used for the given parameter and tends to be somewhat noisy. It is customary to smooth the likelihood function with a Gaussian filter in order to remove noise but the results are sensitive to the width of the filter used. Therefore we choose to plot the cumulative likelihood as this is insensitive to binning and smoothing is not required. We define the cumulative likelihood as follows:

$$I(x) = \frac{\int_{x_{\min}}^{x} \mathcal{L}(y)dy}{\int_{x_{\min}}^{x_{\max}} \mathcal{L}(y)dy}, \qquad (9)$$

where x is the parameter we are interested in and it has a range $x_{\min} \leq x \leq x_{\max}$; $\mathcal{L}(x)$ is the likelihood obtained by marginalizing over other parameters. The central value for the given variable is thus x_c, with $I(x_c) = 0.5$. This can be, and in general it is different from the value of the parameter for maximum likelihood. $I(x)$ is like the cumulative probability function for the parameter x. Parameter values for

which $I(x) = 0.025$ and $I(x) = 0.975$ define the range allowed at 95% confidence limit, i.e. the probability that the variable lies within this range is 0.95. We mark this limit by two vertical lines in all the likelihood plots.

C. The ΛCDM model

Figure 2 shows marginalized cumulative likelihood $I(x)$ for the ΛCDM model, different frames correspond to the different parameters we have considered here. Curves are shown for Ω_{NR}, the shape parameter $\Gamma = \Omega_{NR}h$, Hubble parameter $h = H_0/100 \ \mathrm{kms}^{-1} \ \mathrm{Mpc}^{-1}$, $\Omega_b h^2$, spectral index n, and optical depth to the redshift of reionization τ. The dotted-dashed curves show constraints from WMAP observations of CMB temperature anisotropies; the dotted curve shows constraints from WMAP observations and abundance of rich clusters; the solid curve shows constraints from a combined analysis of WMAP observations, cluster abundance, and high redshift supernovae. The dashed curve shows the constraints from SN observations alone; this has been plotted only for Ω_{NR} as SN data does not constrain other parameters directly. Combined analysis for other parameters does have an input from supernova observations as many models allowed by WMAP and cluster abundance observations are ruled out by SN observations. Vertical lines mark the 95% confidence limit when all the observations are used together. CMB observations allow considerable range for each of these parameters whereas observations of high redshift supernovae provide tight constraints. The reason why SN observations provide a tight constraint is clear from the discussion in the previous section, namely, SN observations favor models with $\Omega_{\mathrm{tot}} \gtrsim 1$. Within the context of models with $\Omega_{\mathrm{tot}} = 1$, SN observations favor models with $w \ll -1$. The ΛCDM
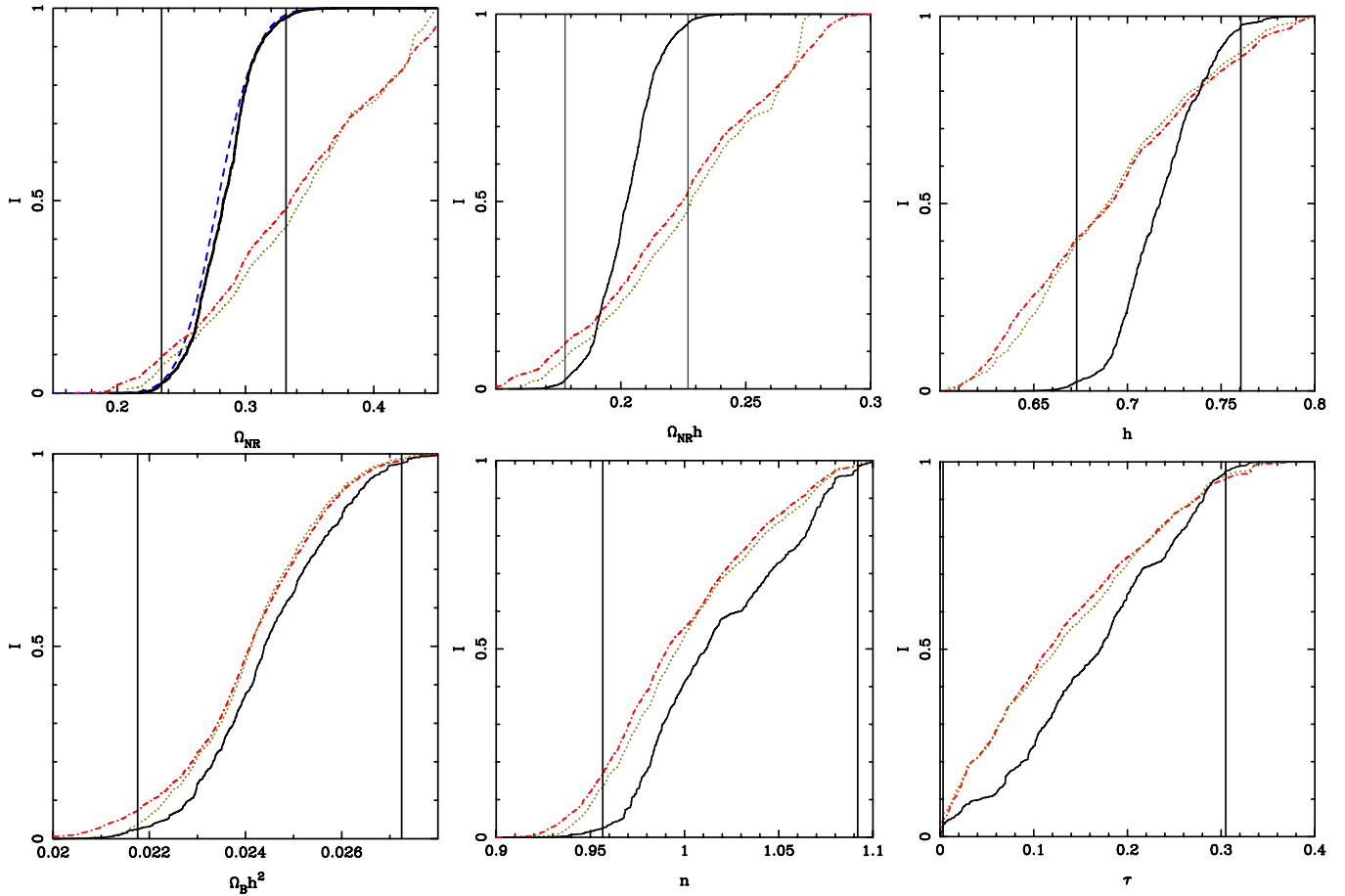
FIG. 2 (color online). This figure shows plots of *I* [see Eq. (9)] for various parameters for the ΛCDM model. The dotted-dashed curves show constraints from the WMAP observations of temperature anisotropies; the dotted curve shows constraints from WMAP observations and abundance of rich clusters; the solid curve shows constraints from a combined analysis of WMAP observations, cluster abundance, and high redshift supernovae. The dashed curve shows the constraints from SN observations alone; this has been plotted only for the relevant parameters. Vertical lines mark the 95% confidence limit for each parameter.

model is only marginally allowed by SN observations within both the sets; flat ΛCDM models are allowed with $\mathcal{P} = 0.12$ [25] and within flat models the ΛCDM model is allowed with $\mathcal{P} = 0.06$.

The allowed range for all the parameters within 68% confidence limit is given in Table III and range allowed in 95% confidence limit is given in Table IV. Table III clearly illustrates the discrepancy between SN observations and WMAP observations. The values are comparable with those obtained in other analyses [5,9]. The range of values for the shape parameter $\Gamma = \Omega_{NR}h$ favored by these observations is consistent with values obtained from galaxy surveys [7,9,69]. The allowed range of values for *h* are in agreement with direct determination [66].

Constraints from abundance of rich clusters do not make a significant impact on the likelihood function of individual parameters even though these constraints reject a significant fraction of models allowed by WMAP observations. To illustrate this, we have plotted points in the Markov chain for ΛCDM models that are allowed by WMAP

observations in a few projections in the parameter space (Fig. 3). Also shown in the same plots are points allowed by abundance of rich clusters of galaxies. This clearly shows that the region in parameter space allowed by cluster abundance is distinctly smaller than that allowed by CMB observations. Well-known degeneracies between parameters are also highlighted by this figure, e.g., there is a clear degeneracy between Ω_{NR} and *h*. An important point to note is that if the preferred range for σ_8 were to be towards larger values than taken here [49,70] then the cluster abundance constraint will favor models with larger Ω_{NR}. There is also a related shift towards $w < -1$.

D. Models with a constant *w*

We now consider models with a constant equation of state parameter *w*. Introduction of this additional parameter changes the relative effectiveness of different observations in constraining cosmological parameters. Observations of high redshift supernovae of type Ia constrain

TABLE III. This table lists the range of relevant parameters allowed within 68% confidence limit from SN, WMAP, WMAP + cluster abundance (CA) requirements and after combining all observations.

Parameter	ΛCDM	w = const	w = const with perturbations	$p = 1$	$p = 2$	
Ω_{NR}	$0.256-0.3$	$0.37-0.47$	$0.37-0.47$	$0.19-0.47$	$0.18-0.47$	SN
	$0.26-0.42$	$0.25-0.37$	$0.28-0.42$	$0.22-0.39$	$0.21-0.37$	WMAP
	$0.265-0.424$	$0.26-0.38$	$0.29-0.43$	$0.24-0.42$	$0.24-0.4$	WMAP + CA
	$0.26-0.3$	$0.27-0.35$	$0.26-0.38$	$0.26-0.35$	$0.3-0.37$	SN + WMAP + CA
w_0		$-1.9--1.39$	$-1.9--1.39$	$-1.89--1.31$	$-1.9--1.33$	SN
		$-1.0--0.67$	$-1.2--0.77$	$-1.19--0.56$	$-1.67--0.7$	WMAP
		$-1.02--0.67$	$-1.13--0.78$	$-1.28--0.56$	$-1.71--0.75$	WMAP + CA
		$-1.41--1.02$	$-1.37--1.04$	$-1.3--1.05$	$-1.69--1.4$	SN + WMAP + CA
$w'(z = 0)$				$-3.2-3.46$	$-3.3-3.99$	SN
				$-0.94-0.67$	$-0.74-4.15$	WMAP
				$-1.0-0.75$	$-1.03-3.94$	WMAP + CA
				$0.21-1.06$	$2.74-4.58$	SN + WMAP + CA

the key cosmological parameters much more strongly than CMB observations for ΛCDM models. This is no longer the case once we introduce w as a parameter. The main reason for this is the degeneracy between w and Ω_{NR}.

In models with $w \neq 1$, it is necessary to take perturbations in the dark energy component into account [68,71,72]. Here, we study models with and without perturbations in dark energy in order to illustrate the role

TABLE IV. This table lists the range of parameters allowed within 95% confidence limit from SN, WMAP, WMAP + cluster abundance requirements and after combining all observations.

| Parameter	ΛCDM	w = const	w = const with perturbations	$p = 1$	$p = 2$	
Ω_{NR}	$0.23-0.33$	$0.27-0.49$	$0.27-0.495$	$0.11-0.49$	$0.11-0.49$	SN
	$0.20-0.45$	$0.16-0.43$	$0.20-0.47$	$0.17-0.45$	$0.18-0.44$	WMAP
	$0.22-0.44$	$0.21-0.42$	$0.22-0.46$	$0.21-0.46$	$0.2-0.44$	WMAP + CA
	$0.23-0.33$	$0.22-0.4$	$0.22-0.4$	$0.21-0.403$	$0.23-0.39$	SN + WMAP + CA
w_0		$-1.97--1.1$	$-1.97--1.1$	$-1.97--1.03$	$-1.97--1.05$	SN
		$-1.39--0.58$	$-1.6--0.63$	$-1.64--0.42$	$-1.93--0.43$	WMAP
		$-1.34--0.63$	$-1.4--0.66$	$-1.73--0.42$	$-1.95--0.47$	WMAP + CA
		$-1.47--0.91$	$-1.48--0.96$	$-1.66--0.97$	$-1.89--1.17$	SN + WMAP + CA
$w'(z = 0)$				$-4.72-4.6$	$-4.73-4.85$	SN
				$-3.09-1.32$	$-2.5-4.87$	WMAP
				$-3-1.35$	$-2.7-4.8$	WMAP + CA
				$-0.38-1.54$	$1.15-4.99$	SN + WMAP + CA
w_{eff} (at LSS)		$-1.4--0.5$		$-1.48--0.59$	$-1.41--0.58$	
$\Omega_b h^2$	$0.02-0.027$	$0.021-0.028$	$0.02-0.027$	$0.02-0.027$	$0.02-0.027$	WMAP
	$0.021-0.027$	$0.022-0.028$	$0.022-0.027$	$0.021-0.027$	$0.022-0.028$	WMAP + CA
	$0.022-0.027$	$0.022-0.027$	$0.022-0.027$	$0.021-0.027$	$0.022-0.028$	SN + WMAP + CA
h	$0.61-0.79$	$0.61-0.78$	$0.6-0.79$	$0.6-0.78$	$0.61-0.78$	WMAP
	$0.61-0.78$	$0.61-0.77$	$0.61-0.78$	$0.61-0.78$	$0.6-0.78$	WMAP + CA
	$0.67-0.76$	$0.67-0.77$	$0.66-0.76$	$0.65-0.75$	$0.64-0.72$	SN + WMAP + CA
τ	$0.002-0.33$	$0.011-0.39$	$0.007-0.35$	$0.13-0.4$	$0.016-0.39$	WMAP
	$0.001-0.32$	$0.028-0.36$	$0.006-0.35$	$0.001-0.37$	$0.015-0.387$	WMAP + CA
	$0.003-0.3$	$0.002-0.29$	$0.022-0.26$	$0.006-0.38$	$0.01-0.39$	SN + WMAP + CA
n	$0.93-1.08$	$0.93-1.1$	$0.93-1.09$	$0.93-1.1$	$0.93-1.09$	WMAP
	$0.94-1.09$	$0.94-1.1$	$0.94-1.09$	$0.94-1.09$	$0.94-1.09$	WMAP + CA
	$0.96-1.09$	$0.94-1.08$	$0.95-1.08$	$0.94-1.09$	$0.93-1.09$	SN + WMAP + CA
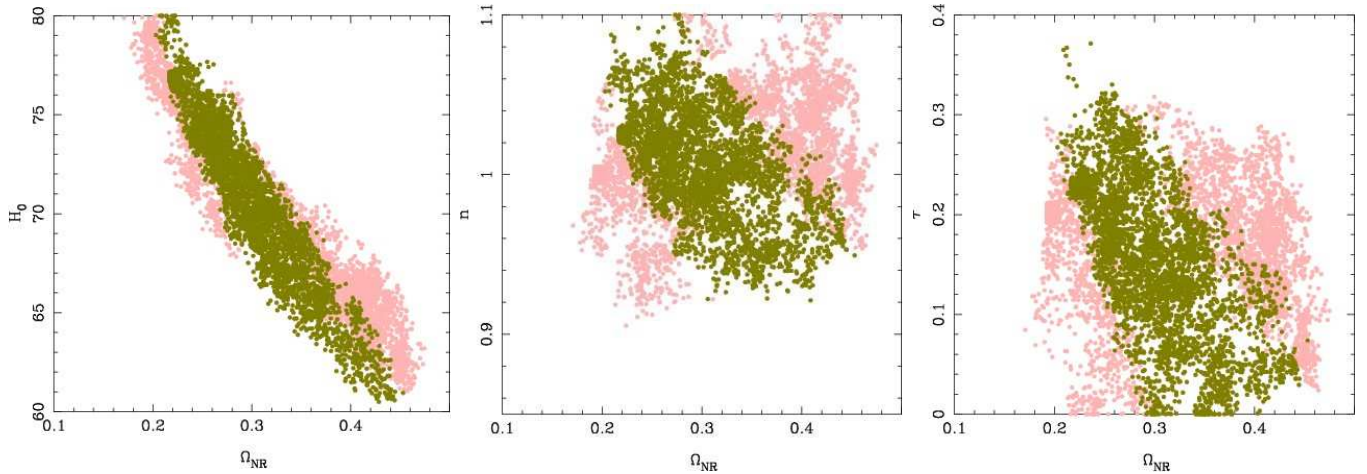
FIG. 3 (color online).   This figure shows points in the Markov chain for ΛCDM models that are allowed by WMAP observations of temperature anisotropies in the CMB within 95% confidence limit in the full parameter space (light points). Models that are also allowed within a 99% confidence limit by abundance of rich clusters of galaxies are shown as dark points. The points are shown in a few projections to illustrate the fact that the requirement of cluster abundance rejects many models allowed by CMB observations. While for some projections it is clear that the region in parameter space allowed by cluster abundance is distinctly smaller than that allowed by CMB observations, in other projections these seem to have an almost complete overlap. This plot also highlights degeneracies in the parameter space.

played by these perturbations and to study how strongly these influence determination of cosmological parameters. Figure 4 shows the likelihood I for parameters Ω_{NR}, w, h, $\Omega_b h^2$, n, and τ in models with and without perturbations in the dark energy component. Models with a larger Ω_{NR} and smaller w are better fits to SN observations, whereas CMB observations prefer models with smaller Ω_{NR} and a larger equation of state parameter w. The combination of these observations and abundance of rich clusters constrains both the parameters to a fairly narrow range, much narrower than is allowed by SN observations alone. Models with $w > -1$ fare badly with CMB observations when perturbations in the dark energy component are taken into account. For models with a constant w, observations allow higher values of $\Omega_b h^2$ than for ΛCDM models. The allowed range in τ is smaller then the case with no dark energy perturbations whereas the ranges for n are similar in both.

We find that the range of w allowed at the 95% confidence limit is smaller when perturbations in dark energy are allowed. For other parameters, the allowed range is similar. In other words, if we ignore perturbations in dark energy we can still make a reasonable estimate of the range of parameters allowed by observations. This fact is of immense use when we work with models that have a varying equation of state parameter w. In order to take full effects of dark energy perturbations in these models it is essential to know full details of the model [68,71]. We cannot include the effect of nonadiabatic perturbations in a model independent study of dark energy models with a varying w. Given the fact that ignoring perturbations in dark energy does not lead to an incorrect estimate of the

range of parameters (except for w) that is allowed, we can safely proceed with our analysis without taking perturbations in dark energy into account. As regards the equation of state parameter w, ignoring perturbations tends to allow $w > -1$ models with a larger probability and we should keep this in mind while interpreting results.

E. Models with varying $w(z)$

We now proceed to the case of varying w, we use two parameterizations given in [24]. The first of these, corresponding to $p = 1$, is a Taylor series expansion for w in scale factor and this is a very commonly used parameterization. The variation of the equation of state parameter is monotonic in this case and rapid increase of w at low redshifts cannot be allowed as it will lead to $w \gtrsim -1/3$ at high redshifts. The parameterization with $p = 2$ avoids this problem to some extent as the value of w at very high redshifts is the same as the present value, but there can be a large deviation from this at low redshifts with the deviation peaking at $z = 1$. Rapid variation at low redshifts has been reported [35] on the basis of SN observations [2,3], and even though these conclusions have been contested [73] it is useful to check if the larger set of observations support a rapid variation of w at low redshifts.

We have already seen in the discussion of fiducial models, supernova observations do not distinguish between models with a constant w and models with a variable equation of state parameter. Also, WMAP observations do not differentiate between the three classes of models being studied here in a statistically significant manner.

Figure 5 shows the allowed ranges of parameters w_0 and $w'(z = 0)$ for $p = 1$ (left panels) and $p = 2$ (right panels).
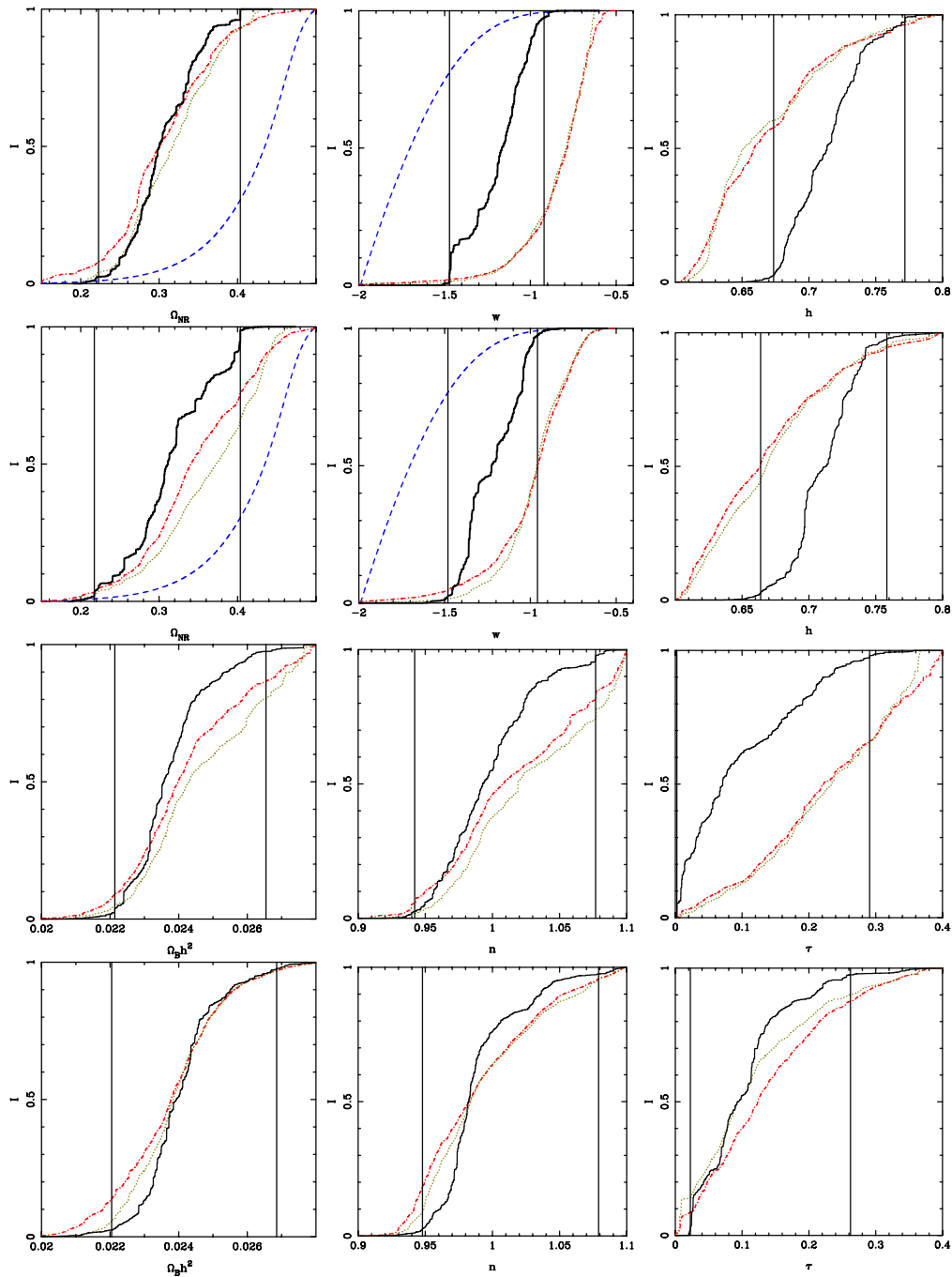
FIG. 4 (color online).   This figure shows I for Ω_{NR}, w, and h for cosmological models with a constant equation of state parameter w. Panels in the first and third row are for models without perturbations in the dark energy component, whereas panels in the second and fourth row are for models with perturbations in dark energy. Each panel shows I derived from observations of high redshift supernovae, WMAP observations, WMAP observations combined with the constraints from abundance of rich clusters, and all three observations in combination (with the same color coding as in Fig. 2). We have marked 95% confidence limits derived from using all the observations in concert as two vertical lines. The relevant parameters are written in the x axis labels of the figures.

In both the parameterizations, the preferred values for w_0 with supernova observations are for phantom models ($w_0 \leq -1$) and a tendency for a larger w at intermediate redshift, i.e., $w_0' \geq 0$ though supernova observations do not provide a clear constraint on this parameter. This is perhaps

related to the fact that there is a strong degeneracy in Ω_{NR} and w_0. CMB observations and abundance of rich clusters of galaxies allow models around the ΛCDM model, which is fairly close to the center of the allowed region. A combination of these three observations rejects models
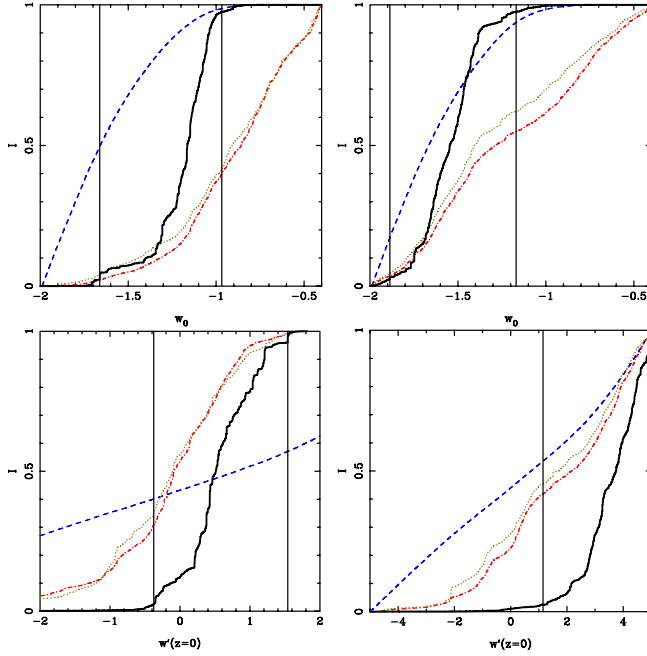
FIG. 5 (color online). This figure shows I for parameters that describe the variation of the equation of state parameter: w_0 and $w'(z = 0)$. Left panels are for $p = 1$ and the right ones are for $p = 2$. Coding used is the same as in Fig. 2.
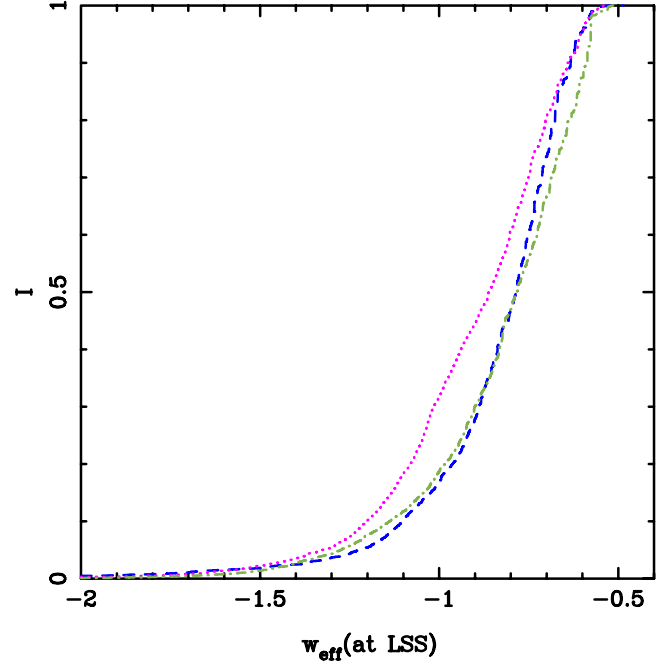

FIG. 6 (color online). This figure shows I for w_{eff} at the redshift of surface of last scattering for the models with constant w (dashed curve), variable w with $p = 1$ (dotted-dashed curve), and with $p = 2$ (dotted curve). Perturbations in dark energy are not taken into account in these models. See text for a more detailed description of this figure.

with $w_0 \ll -1$ due to CMB constraints and $w_0 > -1$ due to SN constraints. Even though all the observations allow $w'_0 = 0$, the combination of these observations does not favor such models. This implies that the overlap of allowed regions for the three observations is stronger for models with $w'_0 \neq 0$; it is clear from Table III that there is no overlap between SN and WMAP at 68% confidence limit for constant w. The ΛCDM model, i.e., $w_0 = -1$ and $w'_0 = 0$ is a marginally allowed model for both the parameterizations.

To understand the nature of constraint from CMB observations [74], we computed the likelihood of w_{eff} [as defined in Eq. (8)] for models by comparing these with WMAP data. This is then compared with the likelihood for w in models with a constant equation of state parameter. We have plotted this in Fig. 6 for $p = 1$ as well as $p = 2$, along with the curve for constant w (with no perturbations in dark energy). All the three curves show very similar behavior and the 95% confidence limit is identical for all three ($-1.5 \leq w_{\text{eff}} \leq -0.6$). This also shows that the CMB observations primarily provide a constraint for w_{eff}. Given that adding perturbations reduces the likelihood for models with $w > -1$, it is likely that detailed analysis of a model with perturbations in dark energy taken into account will limit the range for w_{eff} in this region.

Lastly, we study the effect of varying dark energy on other parameters. The specific question we wish to address is, how the allowed ranges for these parameters change if we allow variation of dark energy. Figure 7 shows like-

lihood for the parameters studied here. We have plotted the likelihood using all three observations for the ΛCDM models, constant w models, as well as for $p = 1$ and $p = 2$. For most parameters, the effect of $w \neq -1$ and varying dark energy is to increase the range of allowed values. This increase in the allowed range is sometimes accompanied by a shift, e.g. for h where varying dark energy models fit observations better with smaller values as compared to the ΛCDM model as well as models with constant w. This shift is primarily due to models with $w > -1$ and this point has been noted in other analyses as well [5]. If this is the case then including perturbations in dark energy may well remove this shift.

Similarly, larger values of spectral index n and optical depth to the epoch of reionization τ fit observations better. As these parameters can be constrained using other observations, we may be able to restrict models with varying w by constraining the values of these parameters. For example, polarization anisotropies in the CMB can be used to constrain τ [59,75]. We find that the presently available information from WMAP about polarization anisotropies does not lead to a significantly improved constraint on the parameter τ.

F. Evolution of dark energy

We now summarize our results for the allowed variation of dark energy, once all three observational constraints
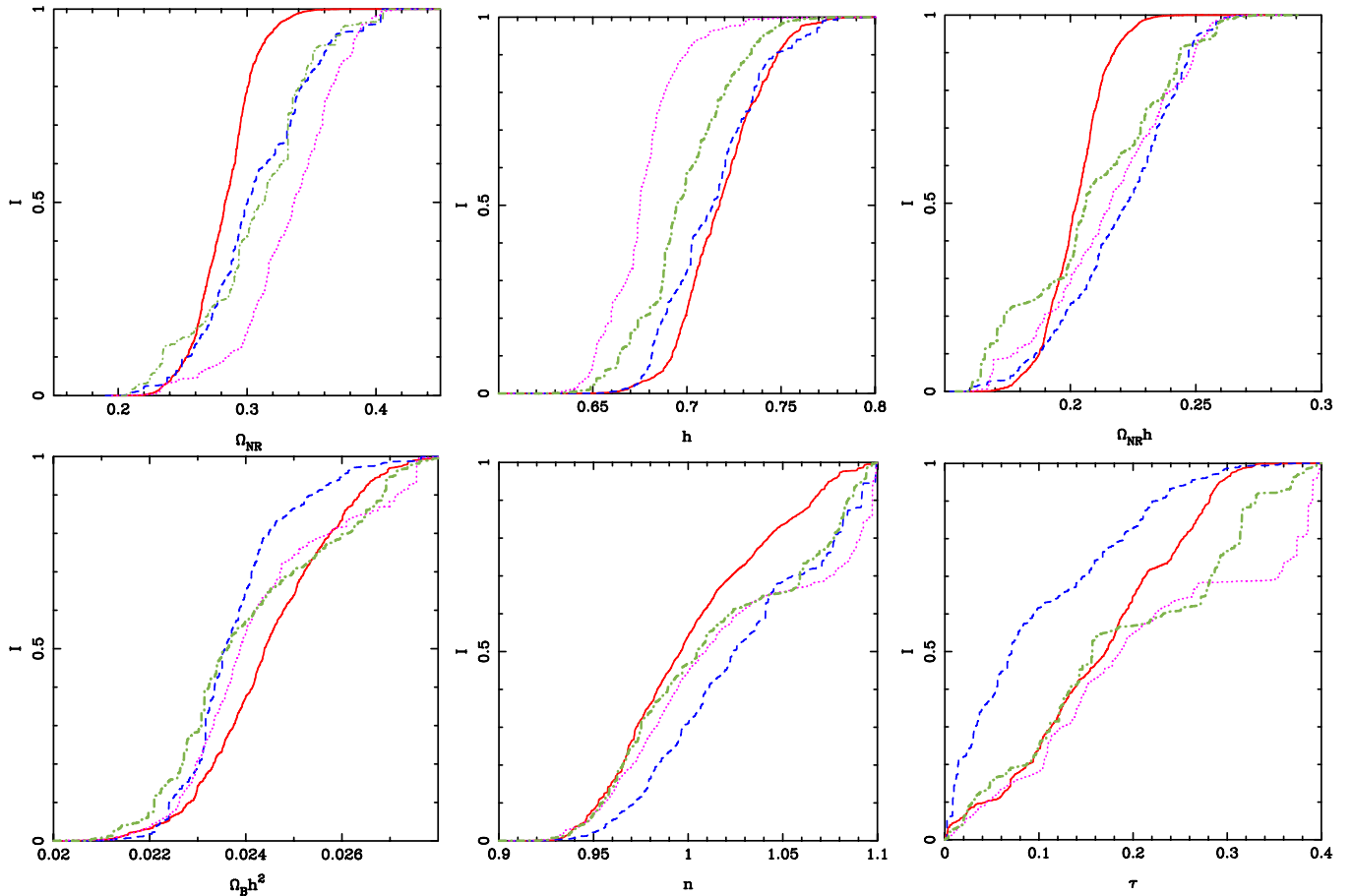
FIG. 7 (color online).   Panels for Ω_{NR}, h, $\Gamma = \Omega_{NR}h$, $\Omega_b h^2$, n, and τ. Solid curve is for ΛCDM, dashed curve for models with constant w, dotted-dashed for $p = 1$, and dotted curve for $p = 2$.

have been taken into account. In the left panel of Fig. 8, we have plotted the cumulative likelihood for the equation of state parameter w at redshift $z = 1$. Here we have used models which lie within the range $-1.1 < w_0 < -0.9$. The upper and lower panels correspond to parameterizations with $p = 1$ and $p = 2$, respectively. The allowed range of variation in the equation of state by supernova observations is much larger than that allowed by WMAP results. This, again, is a reflection of the strong preference of supernova observations for $w \ll -1$ and of the large parameter space allowed by SN data. (Our result that SN data prefers $w \ll -1$ with large variation is consistent with previously published analysis e.g., in [28].) The range of values in both the parameterizations are similar for this subset of models. In the middle panel we have shown the likelihood for variation in the equation of state parameter from the present to its value at redshift $z = 1$. The allowed ranges of variation in dark energy equations of state are different for these two parameterizations. In fact, the constant dark energy equation of state is ruled out at 95% confidence level for $p = 2$ (that is, the probability of occurrence is less than 0.05) when all the constraints are taken into account even though each observational constraint allows such

models individually. Clearly, the models with constant w allowed by each of these observations are ruled out by other observations. The ΛCDM model is allowed for $p = 2$ at 77% C.L. (with probability of 23%) by SN observations and by 0.9% C.L. ($\mathcal{P} = 0.991$) by WMAP observations.

In the right panel, we have shown the ratio of dark energy density at $z = 1$ and the present value. The variation allowed by SN observations is very large, whereas WMAP limits the variation to within a factor 2.5 at 95% confidence limits. This drives the joint analysis to restrict variation even further. That WMAP observations provide a much tighter constraint on the equation of state as compared to SN observations as was shown earlier in [24].

In Fig. 9 we show the allowed range of variation of dark energy as a function of redshift for $w = constant$ models, with and without perturbations at 68%, 95%, and 99% confidence levels. The figure shows the disparity in allowed range by SN observations and WMAP observations at 68% confidence level. Allowing perturbations in dark energy gives a similar range as compared to the case where dark energy perturbations are absent. In Fig. 10 we plot this range for varying dark energy models—top panel for
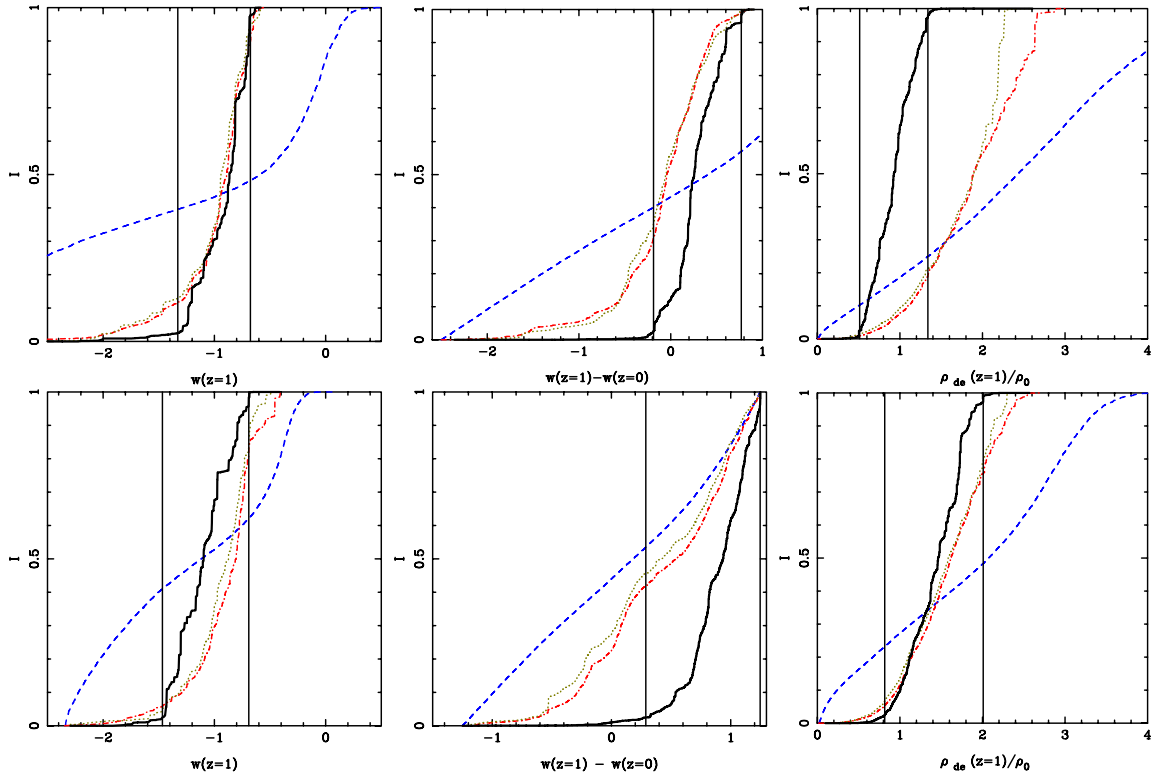
FIG. 8 (color online).　The top and bottom panels in the figure correspond to parameterizations with $p = 1$ and $p = 2$, respectively. The figures on the left show likelihood for the equation of state parameter w at redshift $z = 1$ for models which have equation of state lying within the range $-1.1 < w_0 < -0.9$. In the middle panel we plot the likelihood for variation in the equation of state parameter from the present value at redshift $z = 1$. The third panel shows the allowed range of change in the dark energy density up to $z = 1$. Coding is the same as in Fig. 2.
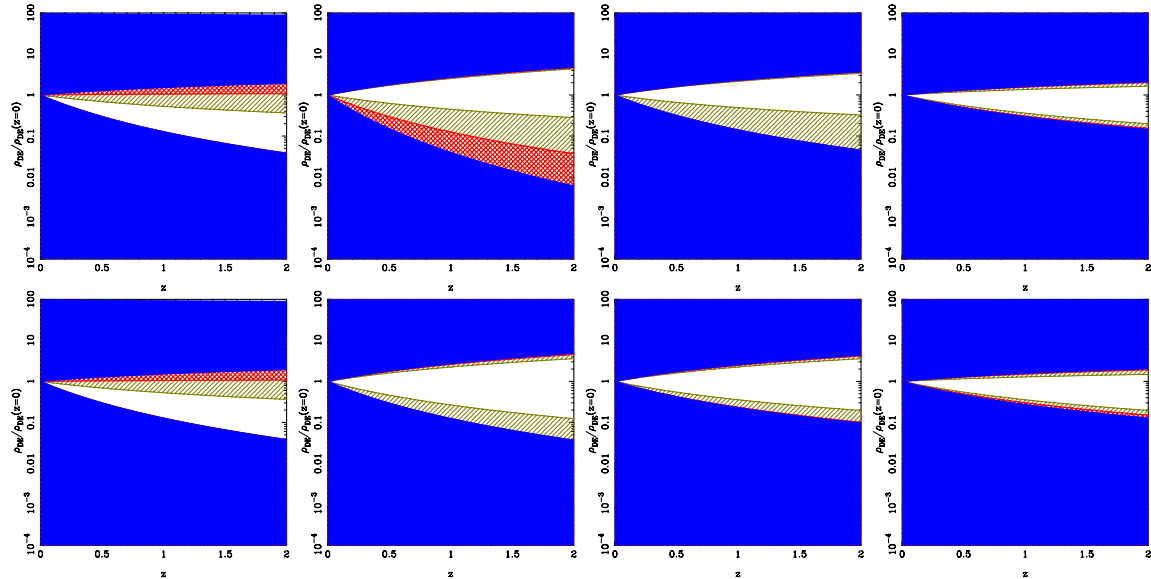

FIG. 9 (color online).　In this figure we plot evolution of dark energy density as a function of redshift. The top panel is for models without dark energy perturbations and the lower panel is with dark energy perturbations included. The left plot in both the rows shows the variation in energy density allowed by supernova observations. The hatched region is excluded at 68% confidence level, crosshatched at 95% confidence level, and solid at 99% confidence level. The white region is the allowed region in variation at 68% significance level. The plot which is second from left (in both the cases) displays the allowed range by WMAP data alone (scheme being the same as in left figure). The next figure shows allowed range by WMAP and cluster abundance observations. The last column shows contribution from combined analysis of the three observations.
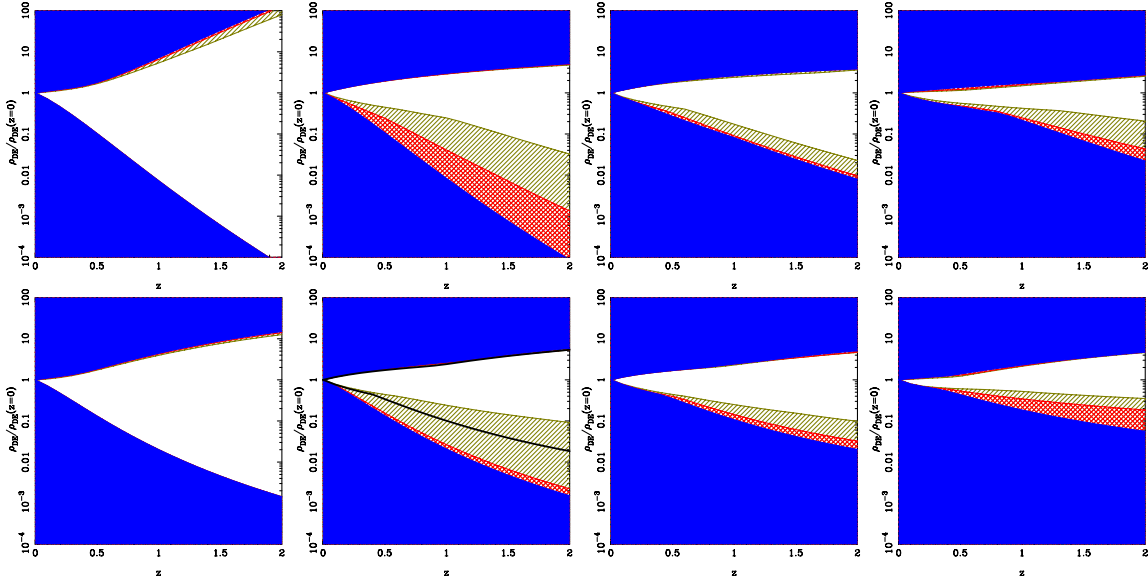
FIG. 10 (color online). Same as Fig. 9 but for varying dark energy models. The top panel is for $p = 1$ and the lower panel is for $p = 2$. Starting from left, the figures show allowed dark energy density variation from SN observations, WMAP observations, WMAP observations combined with cluster abundance requirements and by combined analysis. The region enclosed by solid lines (lower panel, second frame from left) is obtained from the derived constraints on w_{eff}; see text for details.

models with $p = 1$ and lower panel for $p = 2$. As mentioned earlier (see also [24]), SN observations allow a much wider range in change of dark energy density with redshift. The variation allowed by WMAP is smaller in all cases except constant w. The combination of the three constraints allows very little variation, with maximum allowed variation in dark energy density being by a factor 5 up to $z = 2$ at 68% confidence limit. The allowed variation in dark energy density is similar in both the cases, indicating that the constraints on this quantity are parameterization independent to a large extent.

Finally, we would like to make some comments regarding the fact that WMAP constrains the evolution of dark energy more effectively than SN. This arises essentially from the constraint on the angular diameter distance to the last scattering surface, or—equivalently—the effective equation of state parameter w_{eff}. (The integrated Sachs-Wolfe effect and the contribution of other parameters turns out to be less important.) To illustrate this point, we have compared the constraints on dark energy density for $p = 2$ with those implied by constraints on w_{eff}. The second figure in the lower panel in Fig. 10 shows the allowed range in evolution of dark energy density allowed by WMAP data alone for $p = 2$. We have also plotted the allowed range for dark energy density as a function of redshift if $-1.6 \leq w_{\text{eff}} \leq -0.6$, by thick solid lines. This is derived by using all w_0 and w'_0 that lead to w_{eff} in the range given above, and computing the highest and lowest dark energy density amongst this set of models at each redshift. We allow w_0 and w'_0 to vary in the range specified in the priors. The region allowed by the range in w_{eff} and

that directly obtained from all allowed models is similar, with the latter allowing larger variation for phantom models. This reiterates our claim that the main constraint from WMAP data on dark energy parameters is on the value of w_{eff} at the last scattering surface. We believe that the larger range allowed at 95% confidence limit is due mainly to the ISW effect.

V. CONCLUSIONS

In this paper we presented a detailed analysis of constraints on cosmological parameters from different observations. In particular we focused on constraints on dark energy equation of state, its present value, and the allowed range of variation in it.

It is demonstrated that the allowed range for the equation of state parameter w is smaller if dark energy is allowed to cluster. Including perturbations mainly affects models with $w > -1$.

We find that WMAP observations do not distinguish between the ΛCDM model, models with a constant equations of state parameter w, and models with a variable w; the change in χ^2_W for best fit models is less than 3 even as the number of parameters is increased by 3. WMAP allows only a modest variation in energy density of dark energy, with maximum variation being less than a factor of 3 in 99% confidence limit up to $z = 1$. We infer that the main constraint from WMAP observations is for the derived quantity w_{eff}, essentially representing the distance to the last scattering surface.

SN observations favor models with $w < -1$ and $\Omega_{\text{NR}} > 0.4$. A corollary is that if we restrict to models with

$w \geq -1$ then the ΛCDM model is the most favored model. Without this restriction the ΛCDM model is allowed only marginally by the combination of observations used here; this is driven mainly by SN observations.

Allowing variation in dark energy has an impact on other cosmological parameters as the allowed range for many of these parameters becomes larger. Conversely, better measurements of these parameters will allow us to constrain models of dark energy.

We find significant tension between different observations. Our key conclusions in this regard may be summarized as follows:

(i) SN observations favor models with large Ω_{NR} and $w \ll -1$. Indeed, the best fit model is at the edge of our priors.

(ii) Enlarging priors to $0.1 \leq \Omega_{NR} \leq 0.6, \ -0.3 \geq w \geq -3.0$ does not lead to a better fit model for SN observations, indicating that our default priors are sufficiently wide for joint estimation of parameters. This is because $w \ll -1$ is rejected by WMAP observations.

(iii) WMAP observations favor models with $w \sim -1$ with a marginal preference for $w > -1$. Including perturbations in dark energy removes this marginal preference as well.

(iv) For constant w models and models with variable w, the best fit model of each observation is ruled out by the other observations at a high significance level. As an example, the model that best fits the WMAP observations is completely ruled out by SN observations ($\Delta\chi_S^2 = 53$). The problem is slightly less serious if perturbations in dark energy are taken into account ($\Delta\chi_S^2 = 12.5$).

(v) There is overlap of allowed regions at 95% (or better) by these observations, though there is little overlap of allowed regions at 68% confidence limit (see Table III). It can, of course, be argued that situation is not alarming given that there is an overlap of allowed regions in parameter space at 95%. But we find this offset noteworthy.

(vi) Using larger values for σ_8, as indicated by some recent analyses [49,70] favors models with a slightly larger Ω_{NR} and slightly lower w_{eff}.

(vii) Given that the preference of individual observations for different types of models is not understood, and the fact that the best fit model of one is ruled out by the other, it is necessary to use a combination of observations for reliable constraints on models of dark energy. Use of either one of the observations is likely to mislead.

(viii) Our conclusions are not sensitive to priors used for parameters other than Ω_{NR}. Limiting priors for matter density to $0.1 \leq \Omega_{NR} \leq 0.3$ enhances the overlap between SN and WMAP observations and removes the tension between SN and WMAP observations for constant w models.

(ix) If we repeat the analysis of models with variable w with this restricted priors then we find that SN observations strongly favor a variable w as compared to constant w. There is no significant tension between SN and WMAP models in this class of models even for the wider priors, but this is mainly due to a larger number of parameters.

(x) Using only the *Gold* data set for supernovae instead of the *Gold + Silver* used here reduces the tension between the WMAP and supernova observations by a marginal amount.

Given the points noted here regarding tension between different observations, it is important that some effort is made to look for systematic effects in observations as well as in analysis of observations. We have tested our analysis for systematic effects by varying priors and our findings appear to be independent of the chosen priors, the only instance of change in results is mentioned above. Since the SN data set which is used by most people (including in this work) arises from different sources, one needs to be careful regarding hidden systematics (see e.g., the discussion in [76]). When larger, homogeneous SN datasets are available in future (like, for example, from SuperNova Legacy Survey), it is likely that the tension between the SN observations and WMAP results disappear. If it does not, and the agreement continues to exist only at a 3-sigma level, there is some cause for concern.

[1] J. P. Ostriker and P. J. Steinhardt, Nature (London) **377**, 600 (1995); S. D. M. White, J. F. Navarro, A. E. Evrard, and C. S. Frenk, Nature (London) **366**, 429 (1993); J. S. Bagla, T. Padmanabhan, and J. V. Narlikar, Comments Astrophys. **18**, 275 (1996); G. Efstathiou, W. J. Sutherland, and S. J. Maddox, Nature (London) **348**, 705 (1990).

[2] J. L. Tonry *et al.*, Astrophys. J. **594**, 1 (2003); B. J. Barris *et al.*, Astrophys. J. **602**, 571 (2004).

[3] A. G. Riess *et al.*, Astrophys. J. **607**, 665 (2004).

[4] A. Melchiorri *et al.*, Astrophys. J. Lett. **536**, L63 (2000).

[5] D. N. Spergel *et al.*, Astrophys. J. Suppl. Ser. **148**, 175 (2003).

[6] E. Hawkins *et al.*, Mon. Not. R. Astron. Soc. **346**, 78 (2003).

[7] A. C. Pope *et al.*, Astrophys. J. **607**, 655 (2004).

[8] S. L. Bridle, O. Lahav, J. P. Ostriker, and P. J. Steinhardt, Science **299**, 1532 (2003).

[9] M. Tegmark *et al.*, Phys. Rev. D **69**, 103501 (2004).

[10] T. Padmanabhan, gr-qc/0503107.

[11] S. Weinberg, Rev. Mod. Phys. **61**, 1 (1989).

[12] T. Padmanabhan, Phys. Rep. **380**, 235 (2003); P. J. Peebles and B. Ratra, Rev. Mod. Phys. **75**, 559 (2003); V. Sahni and A. Starobinsky, Int. J. Mod. Phys. D **9**, 373 (2000); J. Ellis, Royal Society of London Philosophical Transactions Series A **361**, 2607 (2003); T. Padmanabhan, Curr. Sci. **88**, 1057 (2005).

[13] P. J. Steinhardt, Royal Society of London Philosophical Transactions Series A **361**, 2497 (2003); A. D. Macorra and G. Piccinelli, Phys. Rev. D **61**, 123503 (2000); L. A. Ureña-López and T. Matos, Phys. Rev. D **62**, 081302 (2000); P. F. González-Díaz, Phys. Rev. D **62**, 023513 (2000); R. de Ritis and A. A. Marino, Phys. Rev. D **64**, 083509 (2001); S. Sen and T. R. Seshadri, Int. J. Mod. Phys. D **12**, 445 (2003); C. Rubano and P. Scudellaro, Gen. Relativ. Gravit. **34**, 307 (2002); S. A. Bludman and M. Roos, Phys. Rev. D **65**, 043503 (2002).

[14] C. Armendariz-Picon, V. Mukhanov, and P. J. Steinhardt, Phys. Rev. D **63**, 103510 (2001); T. Chiba, Phys. Rev. D **66**, 063514 (2002); M. Malquarti, E. J. Copeland, A. R. Liddle, and M. Trodden, Phys. Rev. D **67**, 123503 (2003); L. P. Chimento and A. Feinstein, Mod. Phys. Lett. A **19**, 761 (2004); R. J. Scherrer, Phys. Rev. Lett. **93**, 011301 (2004).

[15] T. Padmanabhan, Phys. Rev. D **66**, 021301 (2002).

[16] J. S. Bagla, H. K. Jassal, and T. Padmanabhan, Phys. Rev. D **67**, 063504 (2003); H. K. Jassal, Pramana **62**, 757 (2004); J. M. Aguirregabiria and R. Lazkoz, Phys. Rev. D **69**, 123502 (2004); A. Sen, Phys. Scr., T **117**, 70, (2005); V. Gorini, A. Kamenshchik, U. Moschella, and V. Pasquier, Phys. Rev. D **69**, 123512 (2004); G. W. Gibbons, Classical Quantum Gravity **20**, S321 (2003); C. Kim, H. B. Kim, and Y. Kim, Phys. Lett. B **552**, 111 (2003); G. Shiu and I. Wasserman, Phys. Lett. B **541**, 6 (2002); D. Choudhury, D. Ghoshal, D. P. Jatkar, and S. Panda, Phys. Lett. B **544**, 231 (2002); A. Frolov, L. Kofman, and A. Starobinsky, Phys. Lett. B **545**, 8 (2002); G. W. Gibbons, Phys. Lett. B **537**, 1 (2002); A. Das, S. Gupta, T. Deep Saini, and S. Kar, Phys. Rev. D **72**, 043528 (2005); I. Y. Aref'eva, astro-ph/0410443.

[17] R. R. Caldwell, Phys. Lett. B **545**, 23 (2002); J. Hao and X. Li, Phys. Rev. D **68**, 043501 (2003); G. W. Gibbons, hep-th/0302199; V. K. Onemli and R. P. Woodard, Phys. Rev. D **70**, 107301 (2004); S. Nojiri and S. D. Odintsov, Phys. Lett. B **562**, 147 (2003); S. M. Carroll, M. Hoffman, and M. Trodden, Phys. Rev. D **68**, 023509 (2003); P. Singh, M. Sami, and N. Dadhich, Phys. Rev. D **68**, 023522 (2003); P. H. Frampton, Mod. Phys. Lett. A **19**, 801 (2004); J. Hao and X. Li, Phys. Rev. D **67**, 107303 (2003); P. González-Díaz, Phys. Rev. D **68**, 021303 (2003); M. P. Dabrowski, T. Stachowiak, and M.

Szydłowski, Phys. Rev. D **68**, 103519 (2003); J. M. Cline, S. Jeon, and G. D. Moore, Phys. Rev. D **70**, 043543 (2004); W. Fang, H. Q. Lu, Z. G. Huang, and K. F. Zhang, hep-th/0409080; S. Nojiri and S. D. Odinstov, Phys. Rev. D **72**, 023003 (2005); S. Nesseris and L. Perivolaropoulos, Phys. Rev. D **70**, 123529 (2004); S. Nojiri and S. D. Odinstov, Phys. Rev. D **70**, 103522 (2004); E. Elizalde, S. Nojiri, and S. D. Odinstov, Phys. Rev. D **70**, 043539 (2004); S. Nojiri, S. D. Odinstov, and S. Tsujikawa, Phys. Rev. D **71**, 063004 (2005).

[18] K. Uzawa and J. Soda, Mod. Phys. Lett. A **16**, 1089 (2001); H. K. Jassal, hep-th/0312253; C. P. Burgess, Int. J. Mod. Phys. D **12**, 1737 (2003); K. A. Milton, Gravitation Cosmol. **9**, 66 (2003); P. F. González-Díaz, Phys. Lett. B **481**, 353 (2000).

[19] A. Y. Kamenshchik, U. Moschella, and V. Pasquier, Phys. Lett. B **511**, 265 (2001); N. Bilic, G. B. Tupper, and R. D. Viollier, Phys. Lett. B **535**, 17 (2002); M. C. Bento, O. Bertolami, and A. A. Sen, Phys. Rev. D **66**, 043507 (2002); M. C. Bento, O. Bertolami, and A. A. Sen, Phys. Rev. D **67**, 063003 (2003); M. C. Bento, O. Bertolami, and A. A. Sen, Gen. Relativ. Gravit. **35**, 2063 (2003); M. C. Bento, O. Bertolami, N. M. C. Santos, and A. A. Sen, Phys. Rev. D **71**, 063501 (2005); O. Bertolami, N. M. C. Santos, and A. A. Sen, Mon. Not. R. Astron. Soc. **353**, 329 (2004); A. Dev, D. Jain, and J. S. Alcaniz, Phys. Rev. D **67**, 023515 (2003).

[20] R. Holman and S. Naidu, astro-ph/0408102.

[21] T. Padmanabhan, Classical Quantum Gravity **22**, L107 (2005); I. Shapiro and J. Sola, J. High Energy Phys. 02 (2002) 006; J. Sola and H. Stefancic, Phys. Lett. B **624**, 147 (2005).

[22] T. Padmanabhan and T. R. Choudhury, Phys. Rev. D **66**, 081301 (2002); V. F. Cardone, A. Troisi, and S. Capozziello, Phys. Rev. D **69**, 083517 (2004); P. F. González-Díaz, Phys. Lett. B **562**, 1 (2003); M. A. M. C. Calik, gr-qc/0505035; S. Capozziello, S. Nojiri, and S. D. Odintsov, hep-th/0507182.

[23] V. K. Onemli and R. P. Woodard, Classical Quantum Gravity **19**, 4607 (2002); T. Padmanabhan, Phys. Rep. **406**, 49 (2005); T. Padmanabhan, Classical Quantum Gravity **19**, 5387, (2002); A. A. Andrianov, F. Cannata, and A. Y. Kamenshchik, Phys. Rev. D **72**, 043531 (2005); R. Lazkoz, S. Nesseris, and L. Perivolaropoulos, astro-ph/0503230; M. Szydlowski, W. Godlowski, and R. Wojtak, Astrophys. J. **626**, 657 (2005).

[24] H. K. Jassal, J. S. Bagla, and T. Padmanabhan, Mon. Not. R. Astron. Soc. **356**, L11 (2005).

[25] T. R. Choudhury and T. Padmanabhan, Astron. Astrophys. **429**, 807 (2005).

[26] U. Seljak *et al.*, Phys. Rev. D **71**, 103515 (2005).

[27] Y. Wang, V. Kostov, K. Freese, J. A. Frieman, and P. Gondolo, J. Cosmol. Astropart. Phys. 12 (2004) 003.

[28] B. A. Bassett, P. S. Corasaniti, and M. Kunz, Astrophys. J. Lett. **617**, L1 (2004).

[29] S. Lee, Phys. Rev. D **71**, 123528 (2005).

[30] M. Li, Phys. Lett. B **603**, 1 (2004).

[31] S. Hannestad and E. Mörtsell, J. Cosmol. Astropart. Phys. 9 (2004) 1.

[32] M. Chevallier and D. Polarski, Int. J. Mod. Phys. D **10**, 213 (2001); E. V. Linder, Phys. Rev. Lett. **90**, 091301

(2003).

[33] M. Hamuy *et al.*, Astrophys. J. **112**, 2408 (1996); A. G. Riess *et al.*, Astron. J. **116**, 1009 (1998); S. Perlmutter *et al.*, Astrophys. J. **517**, 565 (1999); A. G. Riess *et al.*, Astron. J. **117**, 707 (1999); A. G. Riess *et al.*, Astrophys. J. **560**, 49 (2001); R. A. Knop *et al.*, Astrophys. J. **598**, 102 (2003); P. M. Garnavich *et al.*, Astrophys. J. **509**, 74 (1998).

[34] T. Padmanabhan and T. R. Choudhury, Mon. Not. R. Astron. Soc. **344**, 823 (2003).

[35] U. Alam, V. Sahni, T. Deep Saini, and A. A. Starobinsky, Mon. Not. R. Astron. Soc. **344**, 1057 (2003); U. Alam, V. Sahni, and A. A. Starobinsky, J. Cosmol. Astropart. Phys. 6 (2004) 8.

[36] Y. Wang and M. Tegmark, Phys. Rev. Lett. **92**, 241 302 (2004); Y. Wang, New Astron. Rev. **49**, 97 (2005).

[37] D. Eisenstein and M. White, Phys. Rev. D **70**, 103523 (2004).

[38] A. S. Friedman and J. S. Bloom, astro-ph/0502559; O. Bertolami and P. T. Silva, astro-ph/0507192.

[39] D. J. Eisenstein, *et al.*, astro-ph/0501171.

[40] Z.-H. Zhu, Mod. Phys. Lett. A **15**, 1023 (2000); N. Sarbu, D. Rusin, and C.-P. Ma, Astrophys. J. **561**, L147 (2001); K. Yamamoto, Y. Kadoya, T. Murata, and T. Futamase, Prog. Theor. Phys. **106**, 917 (2001); M. Sereno, Astron. Astrophys. **393**, 757 (2002); M. Kuhlen, C. R. Keeton, and P. Madau, Astrophys. J. **601**, 104 (2004); A. M.. Lopes and L. Miller, Mon. Not. R. Astron. Soc. **348**, 519 (2004); D.-M. Chen, Astron. Astrophys. **418**, 387 (2004); E. V. Linder, Phys. Rev. D **70**, 043534 (2004); M. Meneghetti, M. Bartelmann, K. Dolag, F. Perrotta, C. Baccigalupi, L. Moscardini, and G. Tormen, New Astron. Rev. **49**, 111 (2005); A. V. Macciò, Mon. Not. R. Astron. Soc. **361**, 1250 (2005).

[41] D. Huterer, Phys. Rev. D **65**, 063001 (2002); M. Bartelmann, F. Perrotta, and C. Baccigalupi, Astron. Astrophys. **396**, 21 (2002).

[42] D. Munshi and Y. Wang, Astrophys. J. **583**, 566 (2003).

[43] N. N. Weinberg and M. Kamionkowski, Mon. Not. R. Astron. Soc. **341**, 251 (2003).

[44] K. Abazajian and S. Dodelson, Phys. Rev. Lett. **91**, 041 301 (2003).

[45] B. Jain and A. Taylor, Phys. Rev. Lett. **91**, 141 302 (2003); G. Bernstein and B. Jain, Astrophys. J. **600**, 17 (2004); R. Massey, A. Refregier, and J. Rhodes, astro-ph/0403229; L. Knox, A. Albrecht, and Y. S. Song, astro-ph/0408141.

[46] K. Benabed and F. Bernardeau, Phys. Rev. D **64**, 083501 (2001); L. Amendola, Phys. Rev. D **69**, 103524 (2004); S. Dedeo, R. R. Caldwell, and P. J. Steinhardt, Phys. Rev. D **67**, 103509 (2003).

[47] S. Borgani, P. Rosati, P. Tozzi, and C. Norman, Astrophys. J. **517**, 40 (1999).

[48] P. T. P. Viana and A. R. Liddle, Mon. Not. R. Astron. Soc. **281**, 323 (1996); T. Kitayama and Y. Suto, Astrophys. J. **469**, 480 (1996).

[49] E. Rasia, P. Mazzotta, S. Borgani, L. Moscardini, K. Dolag, G. Tormen, A. Diaferio, and G. Murante, Astrophys. J. Lett. **618**, L1 (2005).

[50] P. Vielva, E. Martinez-Gonzalez, and M. Tucci, astro-ph/0408252; P. S. Corasaniti, B. A. Bassett, C. Ungarelli, and E. J. Copeland, Phys. Rev. Lett. **90**, 091 303 (2003); P. S.

Corasaniti, M. Kunz, D. Parkinson, E. J. Copeland, and B. A. Bassett, Phys. Rev. D **70**, 083006 (2004); B. Gold, Phys. Rev. D **71**, 063522 (2005).

[51] K. Yamamoto, B. A. Bassett, and H. Nishioka, Phys. Rev. Lett. **94**, 051 301 (2005); T. Matsubara and A. S. Szalay, Phys. Rev. Lett. **90**, 021 302 (2003).

[52] M. O. Calvão, J. R. de Mello Neto, and I. Waga, Phys. Rev. Lett. **88**, 091 302 (2002).

[53] S. Perlmutter, M. S. Turner, and M. White, Phys. Rev. Lett. **83**, 670 (1999); M. Kunz, P. S. Corasaniti, D. Parkinson, and E. J. Copeland, Phys. Rev. D **70**, 041301 (2004).

[54] C. Alcock and B. Paczynski, Nature (London) **281**, 358 (1979).

[55] J. Weller and R. A. Battye, New Astron. Rev. **47**, 775 (2003); J. J. Mohr, astro-ph/0408484; J. Weller, R. A. Battye, and R. Kneissl, Phys. Rev. Lett. **88**, 231 301 (2002).

[56] H. V. Peiris and D. N. Spergel, Astrophys. J. **540**, 605 (2000); P. Fosalba, E. Gaztañaga, and F. J. Castander, Astrophys. J. Lett. **597**, L89 (2003); R. Scranton, *et al.*, astro-ph/0307335; N. Afshordi, Phys. Rev. D **70**, 083536 (2004); N. Padmanabhan, C. M. Hirata, U. Seljak, D. Schlegel, J. Brinkmann, and D. P. Schneider, Phys. Rev. D **72**, 043525 (2005); L. Pogosian, P. S. Corasaniti, C. Stephan-Otto, R. Crittenden, and R. Nichol, astro-ph/0506396.

[57] G. Efstathiou, J. R. Bond, and S. D. M. White, Mon. Not. R. Astron. Soc. **258**, 1 (1992).

[58] D. Huterer and A. Cooray, Phys. Rev. D **71**, 023506 (2005); T. Multamäki, M. Manera, and E. Gaztañaga, Phys. Rev. D **69**, 023004 (2004); A. V. Macciò, S. A. Bonometto, R. Mainini, and A. Klypin, in *Multiwavelength Cosmology.* edited by Manolis Plionis (Kluwer Academic, Dordrecht, The Netherlands, 2004), p. 199; E. V. Linder and A. Jenkins, Mon. Not. R. Astron. Soc. **346**, 573 (2003); D. Pogosyan, J. R. Bond, and C. R. Contaldi, astro-ph/0301310; W. Lee and K. Ng, Phys. Rev. D **67**, 107302 (2003); D. Lee, W. Lee, and K. Ng, Int. J. Mod. Phys. D **14**, 335 (2005); R. Mainini, L. P. L. Colombo, and S. A. Bonometto, astro-ph/0503036; L. Pogosian, J. Cosmol. Astropart. Phys. 4 (2005) 15; D. Rapetti, S. W. Allen, and J. Weller, Mon. Not. R. Astron. Soc. **360**, 555 (2005); J. Shen, B. Wang, E. Abdalla, and R. Su, Phys. Lett. B **609**, 200 (2005); F. Giovi, C. Baccigalupi, and F. Perrotta, Phys. Rev. D **71**, 103009 (2005); G. Chen and B. Ratra, Astrophys. J. Lett. **612**, L1 (2004); P. S. Corasaniti, T. Giannantonio, and A. Melchiorri, Phys. Rev. D **71**, 123521 (2005); R. Jimenez, L. Verde, T. Treu, and D. Stern, Astrophys. J. **593**, 622 (2003); L. Perivolaropoulos, astro-ph/0504582; L. Perivolaropoulos, Phys. Rev. D **71**, 063503 (2005); L. Perivolaropoulos, Phys. Rev. D **70**, 043531 (2004); W. Godlowski and M. Szydlowski, astro-ph/0507322; A. Krawiec, M. Szydlowski, and W. Godlowski, Phys. Lett. B **619**, 219 (2005).

[59] W. Hu and S. Dodelson, Annu. Rev. Astron. Astrophys. **40**, 171 (2002).

[60] M. White and J. D. Cohn, astro-ph/0203120; K. Subramanian, Curr. Sci. **88**, 1068 (2005); M. Giovannini, Int. J. Mod. Phys. D **14**, 363 (2005).

[61] L. Verde *et al.*, Astrophys. J. Suppl. Ser. **148**, 195 (2003).

[62] U. Seljak and M. Zaldarriaga, Astrophys. J. **469**, 437 (1996); http://www.cmbfast.org/.

[63] N. Metropolis, A. W. Rosenbluth, M. N. Rosenbluth, A. H. Teller, and E. Teller, J. Chem. Phys. **21**, 1087 (1953).

[64] A. Lewis and S. Bridle, Phys. Rev. D **66**, 103511 (2002).

[65] A. Gelman and D. B. Rubin, Stat. Sci. **7**, 457 (1992).

[66] W. L. Freedman *et al.*, Astrophys. J. **553**, 47 (2001).

[67] The CMBFAST version (4.5.1) being used here incorporates the effects of perturbations in dark energy for constant w and nonphantom models with a variable $w(z)$.

[68] J. Weller and A. M. Lewis, Mon. Not. R. Astron. Soc. **346**, 987 (2003).

[69] S. Cole *et al.*, Mon. Not. R. Astron. Soc. **362**, 505 (2005).

[70] J. L. Sievers *et al.*, Astrophys. J. **591**, 599 (2003); J. R. Bond *et al.*, Astrophys. J. **626**, 12 (2005).

[71] R. Bean and O. Doré, Phys. Rev. D **69**, 083503 (2004); R. R. Caldwell, R. Dave, and P. J. Steinhardt, Phys. Rev. Lett. **80**, 1582 (1998).

[72] S. Hannestad, Phys. Rev. D **71**, 103519 (2005).

[73] J. Jönsson, A. Goobar, R. Amanullah, and L. Bergström, J. Cosmol. Astropart. Phys. 9 (2004) 7.

[74] T. Deep Saini, T. Padmanabhan, and S. Bridle, Mon. Not. R. Astron. Soc. **343**, 533 (2003).

[75] M. Kaplinghat, M. Chu, Z. Haiman, G. P. Holder, L. Knox, and C. Skordis, Astrophys. J. **583**, 24 (2003); L. P. L. Colombo, J. Cosmol. Astropart. Phys. 3 (2004) 3.

[76] S. Perlmutter and B. P. Schmidt, astro-ph/0303428; S. Nobili *et al.*, Astron. Astrophys. **437**, 789 (2005).